**OFFICE OF NAVAL RESEARCH**

Grant or Contract N00014-95-1-0302
PR# 97PR02146-00

Technical Report No. P276

# Electronic Structure of Pyridine-Based Polymers

by

J.W. Blatchford, T.L Gustafson, and A.J. Epstein

Prepared for Publication in

Journal of Chemical Physics

The Ohio State University
Department of Physics
Columbus, OH



September 20, 1997

# REPORT DOCUMENTATION PAGE

Form Approved OMB No. 0704-0188



1. AGENCY USE ONLY (Leave blank)

2. REPORT DATE: 9/20/97

3. REPORT TYPE AND DATES COVERED: Technical

4. TITLE AND SUBTITLE
Electronic Structure of Pyridine-Based Polymers

5. FUNDING NUMBERS
N00014-95-1-0302

6. AUTHOR(S)
J.W. Blatchford, T.L. Gustafson, and A.J. Epstein

7. PERFORMING ORGANIZATION NAMES AND ADDRESS(ES)
Department of Physics
The Ohio State University
174 West 18th Avenue
Columbus, OH 43210-1106

8. PERFORMING ORGANIZATION REPORT NUMBER
P276

9. SPONSORING/MONITORING AGENCY NAME(S) AND ADDRESS(ES)
Office of Naval Research
800 N. Quincy Street
Arlington, VA 22217

10. SPONSORING/MONITORING AGENCY REPORT NUMBER

11. SUPPLEMENTARY NOTES
Prepared for publication in the Journal of Chemical Physics

12a. DISTRIBUTION/AVAILABILITY STATEMENT
Reproduction in whole or in part is permitted for any purpose of the US Government.
This document has been approved for public relearse and sale; its distribution is unlimited.

12b. DISTRIBUTION CODE

13. ABSTRACT (Maximum 200 words)

We present the results of semiempirical quantum chemical calculations on oligomers of poly (*p*-pyridyl vinylene) (PPyV) and poly (*p*-pyridine) (PPy). The presence op a nitrogen heteroatom in the conjugated backbone of these polymers presents a severe breaking of both spatial and charge-conjugation symmetry (CCS), and the addition of nonbonding ($n$) orbitals has potentially major effects on the photophysics of these systems. Geometries are optimized at the PM3 Hartree-Fock level for neutral, singly charged and doubly charged oligomers. We find that the geometric distortions associated with polaron formation are centered on the vinylene linkages in PPyV-based systems and on the interring bonds in the PPy-based systems. We discuss the electronic structure at the PM3 level applying configuration interaction between singly excited states (SCI), and we demonstrate that the lowest-lying ($n \rightarrow \pi^*$) states of the ideal polymer chain are well above the lowest ($\pi \rightarrow \pi^*$) states, predicting strong fluorescence in these systems. Deviations from ideal geometry, however, can lead to substantial ,mixing of the ($\pi \rightarrow \pi^*$) and ($n \rightarrow \pi^*$) manifolds, thereby altering this conclusion. We calculate absorption spectra for neutral, singly charged (polaron), doubly charged (bipolaron) and triplet-state oligomers using the INDO/SCI technique. For PPyV, comparison of oligomers with differing spatial symmetry allows the isolation of the effects of CCS breaking. All calculated spectra are in good agreement with experimental results and indicate that the symmetry breaking due to the nitrogen heteroatom is weak. In particular, the polaron induces a two-peak, in-gap feature into the absorption spectrum and the bipolaron a single-peak feature, as is seen in the analogous all-hydrocarbon polymers.

14. SUBJECT TERMS
Electronic structure, INDO/SCI, pyridine-based polymers

15. NUMBER OF PAGES
47

16. PRICE CODE

17. SECURITY CLASS. OF RPT
Unclassified

18. SECURITY CLASS OF THIS PG.
Unclassified

19. SECURITY CLASS OF ABSTRCT.
Unclassified

20. LIMITATION OF ABSTRACT
Unlimited

# Electronic structure of pyridine-based polymers

J.W. Blatchford,[a] T.L. Gustafson[b] and A.J. Epstein[a,b]

[a] *Department of Physics and* [b] *Department of Chemistry, The Ohio State University, Columbus, OH 43210-1106*

## Abstract

We present the results of semiempirical quantum chemical calculations on oligomers of poly(*p*-pyridyl vinylene) (PPyV) and poly(*p*-pyridine) (PPy). The presence of a nitrogen heteroatom in the conjugated backbone of these polymers presents a potentially severe breaking of both spatial and charge-conjugation symmetry (CCS), and the addition of nonbonding ($n$) orbitals has potentially major effects on the photophysics of these systems. Geometries are optimized at the PM3 Hartree-Fock level for neutral, singly charged and doubly charged oligomers. We find that the geometric distortions associated with polaron formation are centered on the vinylene linkages in PPyV-based systems and on the interring bonds in the PPy-based systems. We discuss the electronic structure at the PM3 level applying configuration interaction between singly excited states (SCI), and we demonstrate that the lowest-lying ($n \rightarrow \pi^*$) states of the ideal polymer chain are well above the lowest ($\pi \rightarrow \pi^*$) states, predicting strong fluorescence in these systems. Deviations from ideal geometry, however, can lead to substantial mixing of the ($\pi \rightarrow \pi^*$) and ($n \rightarrow \pi^*$) manifolds, thereby altering this conclusion. We calculate absorption spectra for neutral, singly charged (polaron), doubly charged (bipolaron) and triplet-state oligomers using the INDO/SCI technique. For PPyV, comparison of oligomers with differing spatial symmetry allows the isolation of the effects of CCS breaking. All calculated spectra are in good agreement

with experimental results and indicate that the symmetry breaking due to the nitrogen heteroatom is weak. In particular, the polaron induces a two-peak in-gap feature into the absorption spectrum and the bipolaron a single-peak feature, as is seen in the analogous all-hydrocarbon polymers.

## I. INTRODUCTION

With the advent of the polymer light-emitting device (LED) [1,2], an understanding of the electronic structure of conjugated polymers has become increasingly important. The system that has received the most attention is poly(*p*-phenylene vinylene) (PPV) and its derivatives, as they are the most promising candidate to date for LED applications [3]. Due to the nature of the electron-phonon interaction in quasi-one-dimensional systems [4], the fundamental *charge* excitations of PPV are the polaron (radical cation/anion) and the bipolaron (dication/dianion). The presence of such an excitation on a PPV chain leads to a destabilization of the levels near the Hartree-Fock bandgap, resulting in two in-gap levels whose occupation depends on the charge of the species. Because of the $C_{2h}$ spatial symmetry of PPV, the polaron and bipolaron produce a two-peak subgap feature and a one-peak subgap feature in the absorption spectrum for the respectively [5]. It is now generally accepted that the fundamental *neutral* excitation of the polymer is an exciton with substantial Coulomb binding energy [6–10]. The excitonic nature of neutral excited states requires the application of correlated models such as those used in quantum chemistry, and many such studies have been reported for oligomeric model systems for PPV [5,9,11–13].

While PPV possesses both charge-conjugation symmetry (CCS) and $C_{2h}$ spatial symmetry, much recent attention has been given to systems in which these symmetries are broken. For PPV, this can be achieved experimentally by the addition of sidegroups to the phenyl ring. Rice and Gartstein have introduced a semi-analytical model for describing the absorption spectrum of these systems based upon excitation of the benzene monomer and the concept of correlation gaps [14–16]. Their model predicts a characteristic four-peak absorption spectrum for broken-CCS systems, with the positions and oscillator strengths of the four peaks determined by microscopic Coulomb parameters. A four-peak spectrum is also predicted by Chandross *et al.* [9] based on calculations within the Pariser-Parr-Pople (PPP) model augmented with single-excitation configuration interaction (SCI). While the number of features predicted is independent of the model considered, the predicted polarization

dependence is different for the two models.

In this paper, we consider the electronic structure of two representative pyridine-based polymers, namely poly(*p*-pyridyl vinylene) (PPyV) and poly(*p*-pyridine) (PPy), shown in Fig. 1. These pyridine-based analogs of PPV and poly(*p*-phenylene) (PPP), respectively, recently have shown promise for LED applications [17–19], and their photophysics shows interesting deviations from that of PPV and PPP [20,21]. In particular, the inclusion of a nitrogen heteroatom in the unit cell of the pyridine-based systems leads to the introduction of nonbonding ($n$) orbitals (from the N lone pair) into the electronic structure, in addition to the the breaking of CCS and spatial symmetry. We assess the role of these modifications in the electronic structure using various neglect-of-differential-overlap (NDO) methods. Such methods have been applied with great success to the study of PPV oligomers by Brédas and co-workers [5,11–13]. We demonstrate that many experimental observations on the pyridine-based systems can be accounted for by our calculations, including the shape of ground-state and photoinduced absorption features, the strong fluorescence properties, and the morphology dependence of intersystem crossing. We further demonstrate that symmetry breaking has little effect on the observed spectra, so that, e.g., the bipolaron possesses a single in-gap absorption feature. We compare our results with other proposed models for broken-symmetry systems.

## II. METHODS

All calculations were performed on a Pentium computer running at 60 MHz using HyperChem, a software package which is commercially available from AutoDesk, Inc. The method of nomenclature used for the oligomers considered in the calculations is demonstrated in Fig. 1. Oligomers are referred to as 'PYnXX' and 'PYVnXX,' where 'n' refers to the number of pyridine rings in the oligomer and 'XX' refers to the regioisomer considered. For the "head-to-tail" (HT) regioisomer, neighboring pyridine rings are oriented in the same direction. For the "head-to-head" (HH) regioisomer, neighboring rings are oriented oppositely.

The geometries of the oligomers were optimized at the PM3 level [22]. Of the three neglect-of-diatomic-differential-overlap methods (MNDO, AM1, PM3), PM3 gave the most accurate geometry for the pyridine ring with respect to STO-3G and 3-21G *ab initio* calculations. In particular, AM1 gave an overly distorted pyridine ring. The neutral (ground-state) and bipolaron geometries were optimized at the restricted Hartree-Fock (RHF) level and the polaron and triplet geometries at the unrestricted Hartree-Fock (UHF) level. The evolution of the ground-state electronic structure was considered at the PM3+SCI RHF level. Absorption spectra were calculated using the INDO/SCI method in the RHF or restricted open-shell Hartree Fock (ROHF) approximation. The 'ZINDO/S' parameterization of INDO was used [23], as is appropriate for spectroscopic calculations. The size of the CI space was varied with oligomer size, as is discussed below. Experimental spectra were simulated based on the calculated oscillator strengths, $f$, and transition energies, $E_0$, using a Gaussian broadening: $f \cdot \exp[-(E - E_0)^2/2\sigma^2]$, with $\sigma = 0.15$ eV (unless otherwise indicated).

## III. RESULTS

### A. Geometry

Representative bond lengths for a central repeat unit of PM3-optimized PYV6HH and PY6HH are summarized in Fig. 2. While no experimental measurements of these quantities are currently available, the PM3 results are quite similar to those calculated for smaller systems by *ab initio* techniques, and are close to those reported for PPV oligomers [12], with a general shortening of the bonds around the N atom. When allowed to vary, the interring torsion angles between rings in the PPyV oligomers were found to be very small in all cases, reflecting the shallow steric potential in these and related systems [24]. Therefore, to save computational time, geometries for PPyV oligomers were forced to planarity in the calculations. For head-to-head oligomers of PPy, the torsion angle between two facing pyridine rings (e.g., rings 1 and 2 of PY6HH above) was similarly found to be essentially zero

due to lack of steric effects. Adjacent "back-to-back" rings (e.g., rings 2 and 3 of PY6HH), however, were found to have a total torsion angle of $\sim$ 40 degrees between them (i.e., $\pm$20 degrees as mesured from the undisorted plane). For head-to-tail oligomers of PPy, all rings are found to be separated by $\sim$ 40 degree torsion angles.

The geometry relaxation phenomena involved in the formation of polaronic and triplet states are demonstrated for the PYV6HH and PY6HH electron polaron ($P^-$), electron bipolaron ($BP^{-2}$) and triplet exciton (T) in Fig. 3, where changes in bond-lengths are shown along a path through the backbone of the molecule which contains all of the nitrogen atoms. (The sequence of bonds is shown in inset of the Figure.) Similar distortions are seen in the portions of the rings not contained in this path. The results for hole polarons and bipolarons are very similar and are not shown. The option of geometric relaxation in the singlet excited state was not available with the software used. The geometric distortions are nearly independent of the charge of the species, and are strongly localized to the central two rings and their surrounding bonds. For PYV6HH, the vinylene unit experiences bond-order reversal, with the double bonds becoming longer and the single bonds shorter, and the pyridine ring becomes more quinoid-like. Notably, the polaron produces the weakest geometric distortion, as also is seen in PPV oligomers [5]. For all species, the greatest geometric distortion is found to occur in the central vinylene unit, again similar to conclusions drawn concerning the PPV polaron [25]. The vinylene-centered polaron explains the lack of any particularly strong vibrations associated with the nitrogen heteroatom in ns and ms photoinduced infrared absorption experiments [26].

Likewise, for PY6HH, all distortions are centered around the central interring bond, with similar large distortions occurring in the two adjacent interring bonds. The shortening of these bonds, together with an observed planarization of the molecule, reflect aromatic-to-quinoid conversion upon polaron or triplet formation [27]. For both oligomers, the extent of the topological defect induced by the polaron or triplet state is four to six rings, again similar to the results for PPV oligomers [5].

To demonstrate that these conclusions are not merely the result of the symmetry of

the molecule, similar results are displayed for PYV5HT and PY5HT in Fig. 4. Again, the changes in bond-length are shown through a path which includes all of the nitrogens. As with the "hexamers," a vinylene-centered polaron is found for the PPyV oligomer, and the distortions in the PPy oligomer are centered on the two central interring bonds. Both the magnitude and extent of the geometric distortions are similar to the hexamer case, as well as to the results found for PPV [5].

### B. Electronic structure of neutral oligomers

To facilitate the discussion of the electronic structure calculations, the Hückel $\pi$-bandstructures of PPyV and PPy are shown in Fig. 5. This simplistic calculation was performed assuming a single hopping integral $t$ and a nitrogen site energy $\varepsilon_N = \varepsilon_C - 0.5t$ [22]. A head-to-tail geometry was assumed in both cases (so that the unit cell contains a single pyridine ring), and the PPy polymer was assumed to be planar. Nonplanarity of PPy merely results in a narrowing of the calculated Hückel bands. The PPyV bandstructure contains four occupied $\pi$ bands (1-4) and four unoccupied $\pi^*$ bands (1*-4*), as shown. The PPy bandstructure contains three occupied and three unoccupied $\pi-$bands. The $\sigma$-bandstructures for the polymers are not shown, but likely overlap with the outermost $\pi$-bands based on the HF calculations. A band of states from the occupied nonbonding ($n$) levels, is also not shown, but presumably lies close to the uppermost occupied $\pi$ band (1). Each occupied band is approximately mirrored by an unoccupied (starred) band, indicating that PPyV and PPy are nearly charge-conjugation symmetric within this simplistic model.

In PPV and PPP, the $\pi$-levels can be divided into "localized" and "delocalized" orbitals [9]. The localized orbitals derive from benzene molecular orbitals which lack density at the *para* sites along which the polymer is connected. Therefore, both PPP and PPV possess one dispersionless occupied band ($l$) and one dispersionless unoccupied band ($l^*$). The corresponding bands in PPyV are those labelled 2 and 2* in the Figure; interaction with the delocalized bands gives these bands a nonvanishing dispersion in PPyV. In PPP, each

localized band is accidentally degenerate with a delocalized band at $k = \pi/2a$; in PPy, these accidental degeneracies are broken, leading to well-dispersed occupied (1,2) and unoccupied ($1^*$, $2^*$) bands.

In the SCI calculations presented below, the CI space was taken to include transitions from levels corresponding to the occupied bands 1, 2, 3 and $n$ to levels corresponding to the unoccupied bands $1^*$, $2^*$ and $3^*$ of PPyV. For PPy oligomers, transitions from bands 1, 2 and $n$ to bands $1^*$ and $2^*$ were considered. At the HF level, the $\pi$ bands 4 and $4^*$ of PPyV and 3 and $3^*$ of PPy are found to be strongly intermingled with $\sigma$ bands and are difficult to account for. Nevertheless, calculations on PYV2HH and PY2HH which include all of the $\pi$ electrons suggest that the contributions of the outermost bands to the CI are minimal.

We now consider the evolution of the electronic structure with oligomer length. We first consider the results of SCI calculations performed on top of the PM3 calculations. Since we are considering only single excitations, the many-electron states calculated from the CI can be labeled as $(o \rightarrow u)^{2S+1}$, where $o$ and $u$ describe the occupied state and unoccupied state, respectively, from which the transition is derived, and $2S+1$ represents the spin multiplicity of the final state (singlet or triplet). Four categories are allowed depending on the occupied state from which the electron is transferred and on the spin multiplicity: $(\pi \rightarrow \pi^*)^{1,3}$ states derive from promotion of an electron from an occupied $\pi$ level to an unoccupied $\pi^*$ level; $(n \rightarrow \pi^*)^{1,3}$ states derive from the promotion of an electron from a nonbonding state. Note that all nonbonding states are occupied in both polymers. In planar PPyV, the four categories of states are rigorously forbidden to mix. In PPy, however, the nonplanarity of the ground-state molecule can lead to substantial mixing of $(\pi \rightarrow \pi^*)$ and $(n \rightarrow \pi^*)$ manifolds. Nevertheless, even with 40 degree torsion angles between rings, the orbitals of PPy oligomers still largely retain their $(n \rightarrow \pi^*)$ and $(\pi \rightarrow \pi^*)$ characters, thus allowing an approximate categorization of the levels.

Of extreme importance for luminescence in a molecule containing $n$ electrons is the relative position of the lowest $(n \rightarrow \pi^*)$ states with respect to the lowest singlet $(\pi \rightarrow \pi^*)$ state. This is because intersystem crossing (i.e., singlet-to-triplet conversion) between

$(n \rightarrow \pi^*)$ and $(\pi \rightarrow \pi^*)$ states is allowed to first order in the spin-orbit interaction [28]. Therefore, molecules in which an $(n \rightarrow \pi^*)$ state lies below the lowest $(\pi \rightarrow \pi^*)^1$ state generally fluoresce only weakly, if at all.

Figure 6 demonstrates the evolution of the lowest $(\pi \rightarrow \pi^*)$ and $(n \rightarrow \pi^*)$ states of PPyV and PPy oligomers as a function of oligomer length. Here, $m$ refers to the number of non-hydrogen atoms in a path connecting the two ends of the oligomer. Note that these calculations were performed on head-to-head oligomers in hopes of maximizing the interaction between the $n$ levels. The $(n \rightarrow \pi^*)$ states show very little evolution with chain length, a result which can easily be rationalized due to the localized nature of the $n$ level. Also, the singlet-triplet splitting is small for these levels, as is characteristic of molecular systems [29]. On the other hand, the $(\pi \rightarrow \pi^*)$ states exhibit strong evolution with chain length. The position of the various states in the polymer can be estimated via the *ansatz* [30]

$$E_{oligomer}(m) = E_{polymer} + \frac{A}{m}, \tag{1}$$

where $A$ is a constant. The polymer levels therefore correspond to the y-intercepts in Fig. 6. The experimentally determined location of the lowest $(\pi \rightarrow \pi^*)^1$ state [26] is indicated by the arrow in the Figure, and is seen to be in good agreement with the predicted value. For PPyV, it is clear that the lowest $(n \rightarrow \pi^*)$ levels lie well above the lowest $(\pi \rightarrow \pi^*)^1$ level, therefore predicting strong fluorescence for this system. For PPy, the $(n \rightarrow \pi^*)$ levels are significantly closer to, yet still above, the lowest $(\pi \rightarrow \pi^*)^1$ level.

In comparing the results of different-length oligomers, it is imperative that the CI space is kept *size consistent* [22]. Thus the number of levels included in the CI calculation must increase in proportion with the length of the oligomer. The calculated results correspond to CI spaces of size $2N + 1$, where $N$=7 $\times$ 5 for the dimer, 15 $\times$ 11 and 23 $\times$ 17 for the PPyV hexamer. The full calculation for the hexamer was actually too large for the computer to handle, so the CI space was taken just large enough to give a proper calculation of the $(n \rightarrow \pi^*)$ levels for this oligomer. Note that in a recent calculations for PPV oligomers [12] the position of the lowest triplet state was found not to evolve with chain length, suggesting

that the triplet is localized to a single ring. In the present (size-consistent) calculation for PPyV and PPy, this is not the case: the evolution of the lowest triplet with chain length is almost as strong as that of the lowest singlet.

It should be noted that the results presented in Fig. 6 are for the ideal (geometry-optimized) polymer. When ring-torsional disorder is present, however, the conclusions may be invalid. Indeed, substantial mixing of $(\pi \rightarrow \pi^*)$ and $(n \rightarrow \pi^*)$ levels is seen even in geometry-optimized PY4HH, particularly in higher-lying states, as is demonstrated below. A more dramatic example is that of PY4HH with one of the end rings twisted out of the plane by 90 degrees. In this case, the $n$-like orbital of the rotated ring mixes in roughly equal proportion with the $\pi$-like orbital in the more planar portion of the molecule. The triplet state formed between this composite orbital and the LUMO lies *below* the lowest $(\pi, \pi^*)^1$ state, resulting in a potentially large intersystem crossing rate. Similar conclusions can reached for PPyV oligomers. Experimentally, a morphology-dependent intersystem crossing rate is seen, with triplet generation in disordered powder samples roughly ten times higher than in more-ordered film samples or solutions [20]. We propose the morphology dependence to be due to stronger ring-torsional disorder in powder samples, leading to enhanced triplet generation via $(n \rightarrow \pi^*)$ and $(\pi \rightarrow \pi^*)$ state mixing.

### C. Absorption spectra of neutral oligomers

We now discuss the ground-state absorption spectrum of neutral PPyV and PPy. For these calculations, the INDO/SCI technique was implemented. It is possible to calculate absorption spectra using the PM3 technique followed by an SCI calculation. While the PM3 HF electronic structure is probably a much better description of the actual electronic structure than that obtained from INDO, the PM3+SCI spectra are generally untrustworthy, depending sensitively on the size of the CI space. In particular, PM3+SCI calculations for polaronic and triplet states proved to be unreliable, producing many negative eigenvalues. The INDO/SCI method, however, is parameterized specifically for the reproduction of

spectroscopic results and is much more reliable. Unfortunately, due to the relatively poor description of the HF electronic structure, the oscillator strengths of low-lying transitions are somewhat exaggerated, and the entire spectrum is in general blue-shifted from the experimental result. Previous authors have corrected for these shortcomings by correcting the intensities based on valence-effective Hamiltonian calculations and by scaling the spectrum along the energy axis [5]. We choose to merely present the "raw" INDO/SCI result here.

While the main goal of the following is to reproduce experimental observations, we also attempt to asses the role of both spatial and CCS breaking in optical spectra. In general, violations of either symmetry will lead to shifting of oscillator strengths and the appearance of new transitions in optical spectra. Ideally, one could assess the role of CCS breaking by examining the CI coefficients associated with various transitions. For example, if PPyV were charge-conjugation symmetric, then transitions between Hückel bands 1 and $2^*$ of Fig. 5 would have corresponding degenerate transitions between bands 2 and $1^*$. Therefore, any CI expansion which contains contributions from a $1 \rightarrow 2^*$ transition should necessarily contain an *equal* contribution from a $2 \rightarrow 1^*$ transition, and the extent to which one transition is favored over the other in the CI expansion should be a manifestation of CCS breaking.

Unfortunately, it is a general failing of NDO techniques that the HF electronic structure is not charge-conjugation symmetric *even in charge-conjugation symmetric systems such as PPV oligomers.* This conclusion is evidenced by our own results on PPV and PPP oligomers, which reproduce the results of Cornil *et al.* [11]. Similar phenomena have been ascribed to the poor description of the unoccupied levels at the INDO level [5]. While it is possible that this failing may be compensated by the CI calculation, it is nevertheless impossible to directly assess the role of CCS breaking in the pyridine-based systems by simply examining CI coefficients.

On the other hand, the nature of the PPyV system makes it possible to separate the two symmetries by considering the two regioisomers independently. This is because the head-to-head oligomers retain the $C_{2h}$ spatial symmetry of PPV while demonstrating broken CCS. On the other hand, the head-to-tail oligomers do not possess either symmetry. One can

therefore evaluate the role of CCS breaking by comparing head-to-head spectra with those of PPV oligomers, and the effects of additional spatial symmetry breaking can be assessed by comparing head-to-head and head-to-tail spectra.

Figure 7 shows the calculated absorption spectrum for PYV4HH (upper) and PYV4HT (lower). The two spectra are quite similar, indicating that the spatial symmetry breaking introduced by the nitrogen is minimal. The solid and dashed spectra correspond to Gaussian broadening factors of 0.15 eV and 0.35 eV, respectively. The 0.35 eV-broadened spectra best represent the types of linewidths seen in experiment. These spectra consist of four peaks, labeled I-IV in the Figure, together with a high energy feature (HE). The four-peak spectrum is seen in experiment [31], with the HE peak out of experimental range, and the intensities and positions of the peaks are reproduced well by the calculation to within a scaling factor in energy. In the spectrum, as in experiment, peaks I and IV are most prominent, with peak III merely a shoulder to peak IV.

In comparison with calculated results for PPV tetramers [11], the PYV4HH spectrum contains several extra transitions due to broken CCS. A four-peak absorption spectrum is predicted for polymers with broken CCS in the model of Gartstein *et al.* [15] and within the PPP model calculations of Chandross *et al.* [9]. In the present calculation, the presence of four peaks in the spectrum is intimately related to the choice of broadening parameter used. Indeed, the spectrum under 0.15 eV broadening appears to show at least 6 peaks, in addition to the HE feature. One difficulty arises from finite-size effects: Some of the transitions represented in the tetramer spectrum will disappear in the polymer spectrum due to momentum conservation in the translationally invariant system. If spectra of various length oligomers are compared, it is found that the transitions in the bands labeled I, III and IV are robust–their relative oscillator strengths and positions are relatively independent of oligomer length. The number of transitions in the band labeled II, however, is strongly dependent on oligomer length, indicating the role of finite size effects.

One obvious difference between the two regioisomer spectra is that the head-to-tail spectrum contains many more significant transitions than the head-to-head spectrum. As a

result of the sum rule [32], the total oscillator strength in the two spectra should be the same. Therefore, the average oscillator strength of the transitions in the head-to-tail isomer is somewhat less than that in the head-to-head isomer. This is a manifestation of spatial symmetry breaking due to the nitrogen: the head-to-head isomer is inversion symmetric, whereas the head-to-tail isomer is not. Therefore, there are fewer forbidden transitions in the head-to-tail spectrum. Nevertheless, the general shape of the two spectra are very similar, suggesting spatial symmetry breaking plays only a weak role in the spectrum.

We now consider in detail the origin of the features in the PYV4HH spectrum. It is useful to consider the transitions in terms of the Hückel bandstructure presented above. Comparison of the wavefunctions of the HF molecular orbitals with those expected from the Hückel bandstructure allows direct association of the molecular orbitals of the tetramer with the bands 1-4 and $1^*$-$4^*$ of Fig. 5. Likewise, the nonbonding orbitals of the N atoms can be separated out from the $\pi$ and $\pi^*$ levels. For PYV4HH, the first three unoccupied HF levels correspond to band $1^*$ of the polymer, the next four to $2^*$, and the following four to $3^*$. Note that there may be some ambiguity in this assignment due to the fact that the "tetramer" is two carbons short of four complete unit cells; however, the HF orbitals show a clear distinction between the first three unoccupied orbitals and the next four unoccupied orbitals. A similar level scheme exists for the occupied orbitals, with the four nonbonding orbitals interjected periodically. Within the Hückel theory, one expects the lowest lying transition to result from the $1 \rightarrow 1^*$ transition. Two additional low-energy features are expected due to the $1 \rightarrow 2^*$ and $2 \rightarrow 1^*$ transitions.

Table I shows the squared CI coefficients for the various transitions in the calculated absorption spectrum. For ease of presentation, the individual levels involved in the transition are not singled out; only the bands between which the transitions occur are indicated. For example, the peak labeled 'I' in the PYV4HH spectrum is largely (81%) due to the HOMO $\rightarrow$ LUMO transition. This result is typical of such calculations [11]. Of the remaining 19%, 16% of the oscillator strength of this transition comes from other $1 \rightarrow 1^*$ transitions; e.g., HOMO-1 $\rightarrow$ LUMO+1. The feature labeled 'II' contains a large contribution from $1 \rightarrow 2^*$

and $2 \rightarrow 1^*$, as expected. Note that substantial mixing with the $1 \rightarrow 1^*$ transition occurs in this peak. Peaks 'III' and 'IV' demonstrate strong mixing between various bands. The HE feature originates largely, though not entirely, from transitions involving the 3 and $3^*$ bands. If these bands are left out of the calculation, the HE band disappears from the spectrum, leaving the other bands unchanged. Interestingly, configurations involving bands 3 and $3^*$ also play a substantial role in peaks III and IV.

Both the model of Gartstein *et al.* and the calculations of Chandross *et al.* predict strong mixing between the various Hückel-like bands; therefore, a direct comparison between these models and the present calculations based on CI coefficients is quite difficult. The two models differ substantially, however, in their predictions of the polarization dependence of the various features in the absorption spectrum. In particular, the model of Gartstein *et al.* predicts that peak II is polarized perpendicular to (but in the plane of) the chain; whereas Chandross *et al.* predict polarization along the chain. For this reason, we have tabulated the polarization dependence of the observed features in Table I. Much of the oscillator strength of the peak II is polarized along the chain, as predicted by the PPP calculation. Caution should be taken in this interpretation, however, as finite-size effects may also play a role in the polarization dependence [16].

Finally, before leaving the PYV4HH spectrum, we note that the nonbonding orbitals participate only weakly in the observed features. The lowest-lying ($n \rightarrow \pi^*$) transition occurs at 4.583 eV, and its oscillator strength is less than one percent of that of the first optical transition. Note that its polarization is labeled 'z,' indicating polarization perpendicular to the plane of the molecule. No other ($n \rightarrow \pi^*$) state contributes significantly to the spectrum.

Figure 8 displays the INDO/SCI calculated absorption spectra for the two regioisomers of PY4. Again, the solid line corresponds to a broadening of 0.15 eV and the dashed line to 0.35 eV. The 0.35 eV spectrum best reproduces the experimental linewidths. This spectrum shows two clear peaks, labeled I and II in the Figure, and a high-energy feature, HE. Again, the predicted two-peak spectrum closely reproduces the experimental result [31], with the HE peak out of the range of the experiment.

In PY4HH there are two pairs of coplanar rings with a torsion angle of 40 degrees between them. In PY4HT, all rings have a 40 degree torsion angle between them. The resulting change in delocalization leads to a blueshift in the low-energy feature in going from the head-to-head to the head-to-tail spectrum. Again the two spectra are quite similar suggesting the weakness of spatial symmetry breaking. As in the case of PYV4, the PY4HT spectrum displays a greater number of transitions than the PY4HH spectrum. Note that, however, PY4HH is *not* inversion symmetric due to the 40 degree torsion angle in the center of the molecule. It is possible that the PY4HH molecule is approximately inversion symmetric, however, again leading to a larger number of forbidden transitions than in PY4HT.

Table II shows the squared CI coefficients for PY4HH. Again, we label the levels according to their association with the Hückel bands of Fig. 5. As with PYV4, peak I in the PY4HH spectrum is almost entirely $1 \rightarrow 1^*$. The other features are again strong admixtures of the various transitions. The features in the intermediate region between peaks I and II contain strong contributions from $1 \rightarrow 1^*$, $1 \rightarrow 2^*$, and $2 \rightarrow 1^*$, again as expected from Hückel theory. The feature labeled II contains contributions from $2 \rightarrow 2^*$ and the high-energy side of the $1 \rightarrow 1^*$ transition. The features I, II and HE are robust as the length of the oligomer is changed. The number and size of the features contributing to the region between I and II is dependent on oligomer length, indicating finite-size effects.

It is interesting to note the role of the $(n \rightarrow \pi^*)$ state in the nonplanar PY4HH molecule. One effect of the nonplanarity is to mix the $(n \rightarrow \pi^*)$ and $(\pi \rightarrow \pi^*)$ states. Therefore, many of the transitions in Table II contain contributions from both types of states. As a result of this mixing, the $(n \rightarrow \pi^*)$ states acquire substantial oscillator strength. This is dramatically demonstrated by the first two transitions identified with peak II. Both of these transitions are roughly 50% $(n \rightarrow \pi^*)$ and possess oscillator strengths near unity. Furthermore, the polarization of the $(n \rightarrow \pi^*)$ state is now in the 'plane' of the molecule (defined as passing through the long axis of the molecule and lying halfway between the two planes define by the pairs of rings in PY4HH). On the other hand, some $(\pi \rightarrow \pi^*)$ transitions are now polarized perpendicular to the plane of the molecule (again denoted by 'z' in the Table).

### D. Polarons, bipolarons and triplet excitons

We now turn to a discussion of the absorption spectra of the polaron, bipolaron and triplet exciton. At the HF level, the introduction of a polaron or exciton to a neutral chain results in a destabilization of the HOMO and LUMO levels, bringing them into the HF bandgap. This is represented schematically in Fig. 9. The two levels $l$ and $u$ are split of from the bands 1 and $1^*$, respectively. The Figure demonstrates the case of an electron polaron. For the case of the electron bipolaron, the $u$ level is doubly occupied. For the case of the triplet exciton, both levels are singly occupied. It is interesting to note that destabilization of the levels around the bandgap occurs at the HF level even *before* the molecule is allowed to relax geometrically. The geometric distortion from polaron formation further destabilizes these levels.

The spectra for the electron polaron and bipolaron on PYV4HH and PYV4HT are shown in Fig. 10. The spectra of the two regioisomers are very similar, again indicating that spatial symmetry breaking is weak in the pyridine-based systems. The squared CI coefficients are listed for the head-to-head oligomer in Tables III and IV for the polaron and bipolaron, respectively. From Hückel theory, one expects up to three optical transitions for the electron polaron in charge-conjugation symmetric systems, namely $u \rightarrow 1^*$, $l \rightarrow u$, and $l \rightarrow 1^*$. A fourth transition, $1 \rightarrow u$, is degenerate with the $l \rightarrow 1^*$ transition in charge-conjugation symmetric systems, but can result in an extra feature in non-charge-conjugation symmetric systems. The bipolaron can have up to two in-gap transitions ($u \rightarrow 1^*$, $l \rightarrow 1^*$), independent of CCS. In PPV oligomers, the $l \rightarrow 1^*$ and $1 \rightarrow u$ transitions are forbidden by the $C_{2h}$ spatial symmetry, leading to a two-peak polaron and one-peak bipolaron spectrum [5].

The two-peak polaron and one-peak bipolaron spectral signatures are also seen in the PPyV tetramers. Unlike in the case of PPV, however, in the PPyV oligomers the high-energy polaron feature and the single bipolaron feature are actually composed of several transitions. These transitions are indicated in Tables III and IV. In the head-to-head spectrum, P1 is largely (61%) due to transitions from the upper polaron level to the new LUMO ($u \rightarrow 1^*$),

as expected [33]. Of the two largest transitions which contribute to P2 (1.586 eV and 1.728 eV), only one is the expected $l \rightarrow u$ transition. The second transition is actually the $u \rightarrow 2^*$ transition (1.728 eV). As PYV4HH possesses the same $C_{2h}$ spatial symmetry as PPV oligomers, we suggest that this extra transition results from the breaking of charge-conjugation symmetry. The $l \rightarrow 1^*$ and $1 \rightarrow u$ transitions which are forbidden in PPV oligomers [5] also do not occur in the PYV4HH spectra, consistent with the preservation of $C_{2h}$ spatial symmetry in this oligomer. The absence of a third feature in the head-to-tail spectrum indicates that spatial symmetry breaking is weak. While it is also true that the $l \rightarrow 1^*$ transition is predicted to be weak in systems where polaron confinement is strong [33], we note that the two-peak polaron spectrum can be seen in PPyV oligomers even *before* geometric relaxation is performed. Therefore, we believe that the absence of the third peak is truly due to symmetry considerations, and not due to polaron confinement.

In the bipolaron spectrum, the singular feature in the spectra is due almost entirely (90%) to transitions from the upper bipolaron level to the LUMO ($u \rightarrow 1^*$), as expected [33]. Again, the $l \rightarrow 1^*$ transitions which are forbidden in PPV oligomers [5] do not occur in PPyV oligomers. In particular, a second feature is absent from the head-to-tail spectrum, again suggesting the weak role of spatial symmetry breaking. Again, the single-peak bipolaron spectrum can be recovered in PPyV oligomers *before* geometric relaxation has occurred, indicating that the absence of a second peak is related to the relatively weak spatial symmetry breaking in these systems, and not due to polaron confinement considerations.

We also calculated spectra for hole polarons and bipolarons. The shape of these spectra are similar to those of their electron counterparts (i.e., two-peak polaron spectrum, etc.), with the spectrum of the positively charged entity rigidly redshifted from its negatively charged counterpart by several tenths of an eV. While it is tempting to ascribe this redshift to the broken charge conjugation symmetry in the system, our calculations on PPV oligomers indicate that electron and hole polarons have different spectra even in this charge-conjugation symmetric system. Again, this result can be explained by the poor description of the unoccupied states afforded by the INDO calculation [5].

The polaron and bipolaron spectra are shown for the two regioisomers of PPy in Fig. 11. The squared CI coefficients are presented in Tables V and VI, respectively. The two-peak polaron spectrum and one-peak bipolaron spectrum are reminiscent of PPP oligomers [34], indicating only weak symmetry breaking. The polaron spectra are somewhat more greatly affected by regioregularity; however, the bipolaron spectra are quite similar. For the head-to-head spectra, again the P1 transition is largely (80%) upper-polaron-level to LUMO, as expected. In contrast to the case of PYV4HH, in the PY4HH spectrum P2 contains essentially one transition (2.817 eV) that is 72% $l \rightarrow u$, as expected. Again, the main bipolaron transition (BP1) is almost entirely (92%) $u \rightarrow 1^*$, as expected. Unlike in the case of PYV4, in PY4 the bipolaron possesses a substantial shoulder (BP2). This shoulder is mainly due to transitions to the $2^*$ level. Again, the $l \rightarrow 1^*$ and $1 \rightarrow u$ transitions that are forbidden in PPV oligomers do not contribute to the spectra of the PPy oligomers.

Experimentally, a two-peak feature is seen in the millisecond photoinduced absorption spectrum of both PPyV and PPy, particularly in films [31]. From the discussion above, these spectra are assigned to polaron absorptions; however, exactly which types of polarons (electron or hole, head-to-head or head-to-tail) are present is not determinable from the above considerations. Bipolarons have not been clearly detected in any of the pyridine-based polymers.

The triplet-triplet spectra for PYV4 and PY4 are shown in Figs. 12 and 13, respectively. The squared CI coefficients for the head-to-head oligomers are shown in Tables VII and VIII respectively. Again, the spectra are fairly independent of the regioisomer considered, suggesting a weak role of spatial symmetry breaking. For PPV, it has been indicated that a single strong transition dominates the triplet-triplet spectrum [12]. Our own calculations also indicate a single strong transition in oligomers of PPP. For the triplet in PYV4 and PY4, as with the polaron and bipolaron, the main feature is composed of several transitions, each of which is a strong admixture of various HF configurations. The additional transitions in the PYV4HH spectrum again reflect the breaking of charge-conjugation symmetry in this system. As the triplet spectrum is likely more affected by correlations than the polaron or

bipolaron spectra, it is difficult to compare the observed transitions with those expected from Hückel theory.

Experimentally, a single feature is seen [31] whose position and shape is matched quite well by the PYV4HT spectrum when the results are scaled with the absorption spectra. On the other hand, the PPy triplet-triplet spectrum is observed experimentally to be nearly identical to the PPyV spectrum. This observation is not reproduced by the calculation.

## IV. SUMMARY AND CONCLUSIONS

The role of spatial symmetry breaking in the pyridine-based systems studied is at best weak. This is evidenced by a general lack of dependence of calculated spectroscopic results on the regioisomer considered. In particular, comparison of the two regioisomers of PPyV allows the direct evaluation of spatial symmetry, as the head-to-head oligomers retain the $C_{2h}$ spatial symmetry of PPV oligomers; whereas the head-to-tail oligomers show broken spatial symmetry. For the PPyV oligomers, spatial symmetry breaking leads to additional high-energy, low-oscillator strength transitions in the absorption spectrum of neutral oligomers; however, the general shape of the spectrum is independent of regioisomer. Polaron, bipolaron and triplet spectra are somewhat less affected by spatial symmetry breaking, which results in slight shifts in oscillator strength among the various transitions.

The role of CCS breaking is somewhat more elusive, as the INDO technique generally gives inadequate results even for charge-conjugation symmetric systems. Nevertheless, the effects of CCS breaking in the pyridine-based systems can be isolated by comparing the results for head-to-head oligomers of PPyV with those of PPV, as both possess the same $C_{2h}$ spatial symmetry. Although the breaking of CCS introduces several new transitions in the pyridine-based systems, particularly in the absorption spectrum, in general the spectroscopic properties of the these systems closely resemble those of their hydrocarbon analogues, indicating that CCS breaking is also weak. In particular, the electron polaron introduces two in-gap features into the absorption spectrum of the pyridine-based oligomer, and the

electron bipolaron introduces a single in-gap feature, as predicted for PPV [5]. The general shapes of the calculated absorption spectra for the pyridine-based oligomers are consistent with that expected from theories in which CCS is weakly broken [16].

The ($n$,$\pi^*$) states play a unique role in these systems. The present calculations find these levels too high in energy to affect the photophysics of the ideal geometry-optimized polymer, predicting strong luminescence for these systems. However, nonplanarity can induce mixing of these levels with the ($\pi$,$\pi^*$) states, allowing them to lower their energy and increase their oscillator strength substantially. We therefore predict a morphology dependence to the photophysics, in particular to rates of intersystem crossing.

Indeed, the morphology dependence of intersystem crossing is seen in experiment [31]. Several other experimental observations are predicted well by the current calculations, notably, the four-peak PPyV absorption spectrum, the two-peak PPy absorption spectrum, and the two-peak polaron absorption spectra. In addition, the PPyV triplet-triplet spectrum is well predicted by our calculations. Finally, the vinylene-centered polaron predicted by the calculations is consistent with photoinduced infrared absorption data, which demonstrate a lack of ring-based modes.

This research was supported in part by the Office of Naval Research.

# REFERENCES


[1] J.H. Burroughes, D.D.C. Bradley, A.R. Brown, R.N. Marks, K. Mackay, R.H. Friend, P.L. Burns and A.B. Holmes, Nature **347**, 539 (1990).

[2] D. Braun and A.J. Heeger, Appl. Phys. Lett. **58**, 1982 (1991).

[3] An extensive list of references on polymer LEDs can be found in D. Braun, A. Brown, E. Staring and E.W. Meijer, Synth. Met. **65**, 85 (1994).

[4] A.J. Heeger, S. Kivelson, J.R. Schrieffer and W.P. Su, Rev. Mod. Phys. **60**, 781 (1988).

[5] J. Cornil, D. Beljonne and J.L. Brédas, J. Chem. Phys. **103**, 834 (1995).

[6] U. Rauscher, H. Bassler, D.D.C. Bradley and M. Hennecke, Phys. Rev. B **42**, 9830 (1990).

[7] P. Gomes da Costa and E.M. Conwell, Phys. Rev. B **48**, 1993 (1993).

[8] J.M. Leng, S. Jeglinski, X. Wei, R.E. Benner, Z.V. Vardeny, F. Guo and S. Mazumdar, Phys. Rev. Lett. **72**, 156 (1994).

[9] M. Chandross, S. Mazumdar, S. Jeglinski, X. Wei and Z.V. Vardeny, Phys. Rev. B **50**, 14702 (1994); M. Chandross, S. Mazumdar, M. Liess, P.A. Lane, Z.V. Vardeny, M. Hamaguchi and K. Yoshino, submitted.

[10] M. Yan, L.J. Rothberg, F. Papadimitrakopoulos, M.E. Galvin and T.M. Miller, Phys. Rev. Lett. **72**, 1104 (1994).

[11] J. Cornil, D. Beljonne, R.H. Friend and J.L. Bredas, Chem. Phys. Lett. **223**, 82 (1994).

[12] D. Beljonne, Z. Shuai, R.H. Friend and J.L. Bredas, J. Chem. Phys. **102**, 2042 (1995).

[13] J. Cornil, D. Beljonne, D.A. dos Santos, Z. Shuai and J.L. Bredas, Synth. Met., in press.

[14] M.J. Rice and Y.N. Gartstein, Phys. Rev. Lett. **73**, 2504 (1994).

[15] Y.N. Gartstein, M.J. Rice and E.M. Conwell, Phys. Rev. B **51**, 5546 (1995).

[16] Y.N. Gartstein, M.J. Rice and E.M. Conwell, Phys. Rev. B **52**, 1683 (1995).

[17] D.D. Gebler, Y.Z. Wang, J.W. Blatchford, S.W. Jessen, L.B. Lin, T.L. Gustafson, H.L. Wang, T.M. Swager, A.G. MacDiarmid and A.J. Epstein, J. Appl. Phys. **78**, 4264 (1995).

[18] J. Tian, M.E. Thompson, C. Wu, J.C. Sturm, R.A. Register, M.J. Marsella and T.M. Swager, Polym. Preprints **35**, 761 (1994).

[19] Y.Z. Wang, D.D. Gebler, L.B. Lin, J.W. Blatchford, S.W. Jessen, H.L. Wang and A.J. Epstein, Appl. Phys. Lett. **68**, 894 (1996).

[20] J.W. Blatchford, S.W. Jessen, L.B. Lin, J.J. Lih, T.L. Gustafson, A.J. Epstein, D.K. Fu, M.J. Marsella, T.M. Swager, A.G. MacDiarmid, S. Yamaguchi and H. Hamaguchi, Phys. Rev. Lett. **76**, 1513 (1996).

[21] J.W. Blatchford *et al.*, in *Electronic, Magnetic and Optical Properties of Organic Solid State Materials III*, edited by L.R. Dalton *et al.* (Pittsburg, Materials Research Society, 1996), in press.

[22] For a discussion of the various quantum chemical techniques, see, e.g., I.N. Levine, *Quantum Chemistry* (Englewood Cliffs, Prentice Hall, 1991).

[23] M.C. Zerner, G.H. Loew, R.F. Kichner and U.T. Mueller-Westerhoff, J. Am. Chem. Soc. **102**, 589 (1980).

[24] O. Lhost and J.L. Bredas, J. Chem. Phys. **96**, 5279 (1992).

[25] H.A. Mizes and E.M. Conwell, Synth. Met. **68**, 145 (1995).

[26] J.W. Blatchford, S.W. Jessen, L.B. Lin, J.J. Lih, D.D. Gebler, Y. Wang, T.L. Gustafson, A.J. Epstein, H.L. Wang, T.M. Swager, A.G. MacDiarmid, T. Yuzawa, T. Tahara, S. Yamaguchi and H. Hamaguchi, in *Time-resolved Vibrational Spectroscopy VII*, edited by W.H. Woodruff (Springer Verlag, Berlin), in press.

[27] J.L. Brédas, R.R. Chance and R. Silbey, Phys. Rev. B **26** 5843 (1982).

[28] M. El Sayed, J. Chem. Phys. **38**, 2834 (1963).

[29] R.S. Becker, *Theory and Interpretation of Fluorescence and Phosphorescence* (New York, Wiley Interscience, 1969).

[30] A. Schmidt, M.L. Anderson, D. Dunphy, T. Wehrmeister, K. Müllen and N.R. Armstrong, Adv. Mat. **7**, 722 (1995).

[31] A.J. Epstein, J.W. Blatchford, Y.Z. Wang, D.D. Gebler, S.W. Jessen, L.B. Lin, T.L. Gustafson, D.K. Fu, H.L. Wang, T.M. Swager and A.G. MacDiarmid, Synth. Met. in press (1996).

[32] J.B. Birks, *Photophysics of Aromatic Molecules* (London, Wiley Interscience, 1970).

[33] K. Fesser, A.R. Bishop and D.K. Campbell, Phys. Rev. B **27**, 4804 (1983).

[34] Y. Furukawa, Synth. Met. **69**, 629 (1995).

## FIGURES

FIG. 1. Repeat units for PPyV and PPy; representative oligomers used in this study. Nomenclature is described in the text.

FIG. 2. Bond lengths (in Angstroms) of central repeat unit of neutral PYV6HH (upper) and PY6HH (lower) after PM3 geometry optimization.

FIG. 3. Change in bond length vs. bond number for PYV6HH (upper) and PY6HH (lower). The geometrical distortions are mapped along a path containing all N atoms, as is indicated in the insets.

FIG. 4. Change in bond length vs. bond number for PYV5HT (upper) and PY5HT (lower). The geometrical distortions are mapped along a path containing all N atoms, as is indicated in the insets.

FIG. 5. Calculated Hückel $\pi$-electron structure for PPyV (upper) and PPy (lower).

FIG. 6. Evolution of energies of lowest ($\pi \rightarrow \pi^*$) and ($n \rightarrow \pi^*$) states, calculated at the PM3+SCI level, as a function of inverse oligomer length (in number of carbons) for PPyV (upper) and PPy (lower) head-to-head oligomers. Arrows represent experimentally determined $(\pi \rightarrow \pi^*)^1$ location.

FIG. 7. INDO/SCI calculated absorption spectrum of neutral PYV4HH (upper) and PYV4HT (lower), assuming a 0.15 eV Gaussian broadening (solid lines) or 0.35 eV Gaussian broadening (dashed lines).

FIG. 8. INDO/SCI calculated absorption spectrum of neutral PY4HH (upper) and PY4HT (lower), assuming a 0.15 eV Gaussian broadening (solid lines) or 0.35 eV Gaussian broadening (dashed lines).

FIG. 9. Schematic representation of Hückel levels of an electron polaron on a PPyV chain.

FIG. 10. INDO/SCI calculated absorption spectrum of an electron polaron (solid) and electron bipolaron (dashed) on PYV4HH (upper) and PYV4HT (lower).

FIG. 11. INDO/SCI calculated absorption spectrum of an electron polaron (solid) and electron bipolaron (dashed) on PY4HH (upper) and PY4HT (lower).

FIG. 12. INDO/SCI calculated triplet-triplet absorption spectrum of PYV4HH (upper) and PYV4HT (lower).

FIG. 13. INDO/SCI calculated triplet-triplet absorption spectrum of PY4HH (upper) and PY4HT (lower).

## TABLES

TABLE I. INDO/SCI transitions energies, polarizations, oscillator strengths, and squared CI coefficients for neutral PYV4HH. Polarization represents the angle of the transition dipole (in deg.) in the plane of the molecule with respect to the long axis of the molecule.

TABLE II. INDO/SCI transitions energies, polarizations, oscillator strengths, and squared CI coefficients for neutral PY4HH.

TABLE III. INDO/SCI transitions energies, oscillator strengths, and squared CI coefficients for an electron polaron on PYV4HH.

TABLE IV. INDO/SCI transitions energies, oscillator strengths, and squared CI coefficients for an electron bipolaron on PYV4HH.

TABLE V. INDO/SCI transitions energies, oscillator strengths, and squared CI coefficients for an electron polaron on PY4HH.

TABLE VI. INDO/SCI transitions energies, oscillator strengths, and squared CI coefficients for an electron bipolaron on PY4HH.

TABLE VII. INDO/SCI transitions energies, oscillator strengths, and squared CI coefficients for triplet exciton on PYV4HH.

TABLE VIII. INDO/SCI transitions energies, oscillator strengths, and squared CI coefficients for triplet exciton on PY4HH.

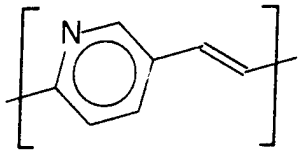

PPyV

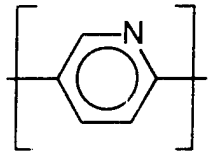

PPy

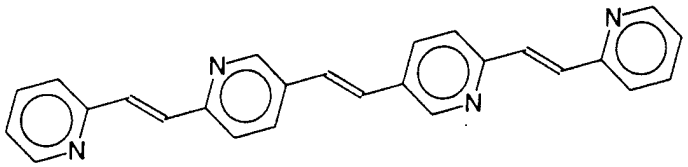

PYV4HH

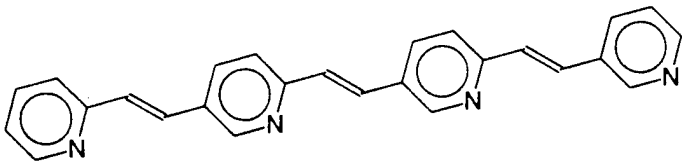

PYV4HT

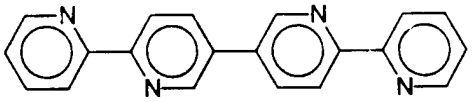

PY4HH

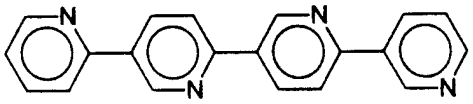

PY4HT

**Figure 1, Blatchford, Gustafson and Epstein**

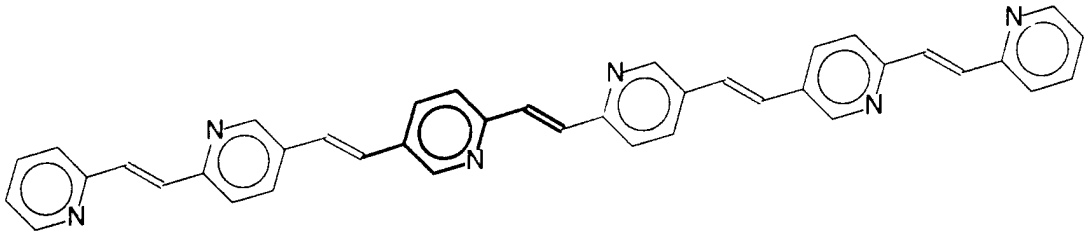


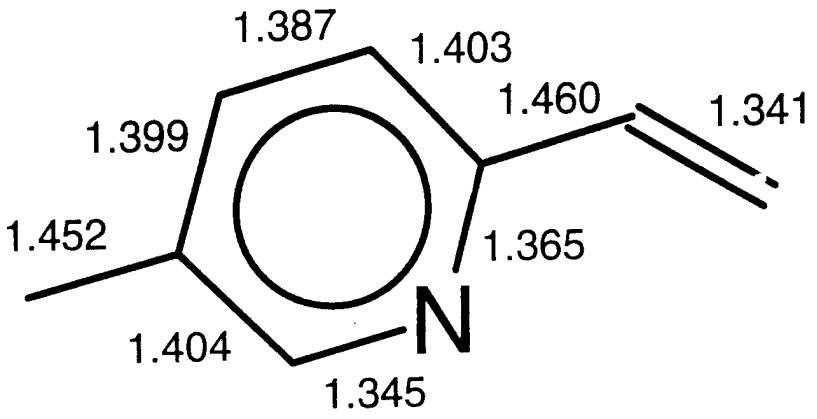


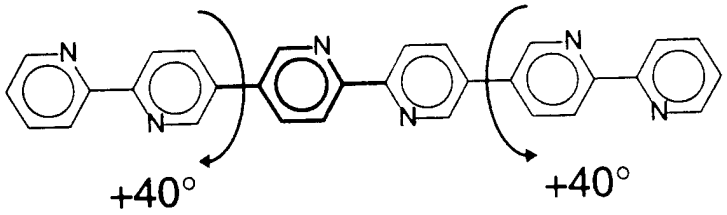


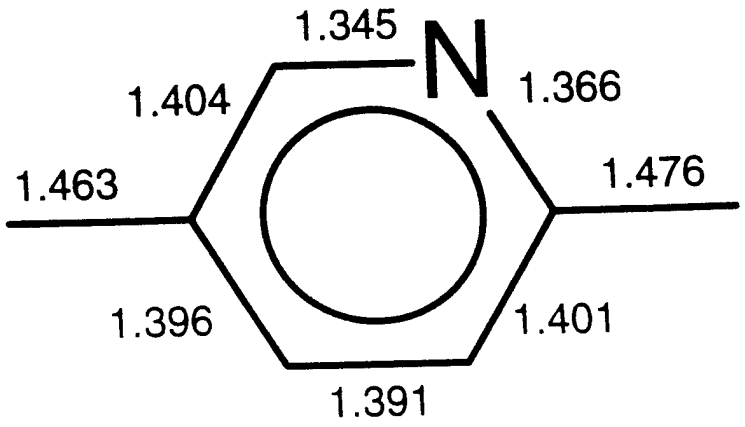


**Figure 2, Blatchford, Gustafson and Epstein**

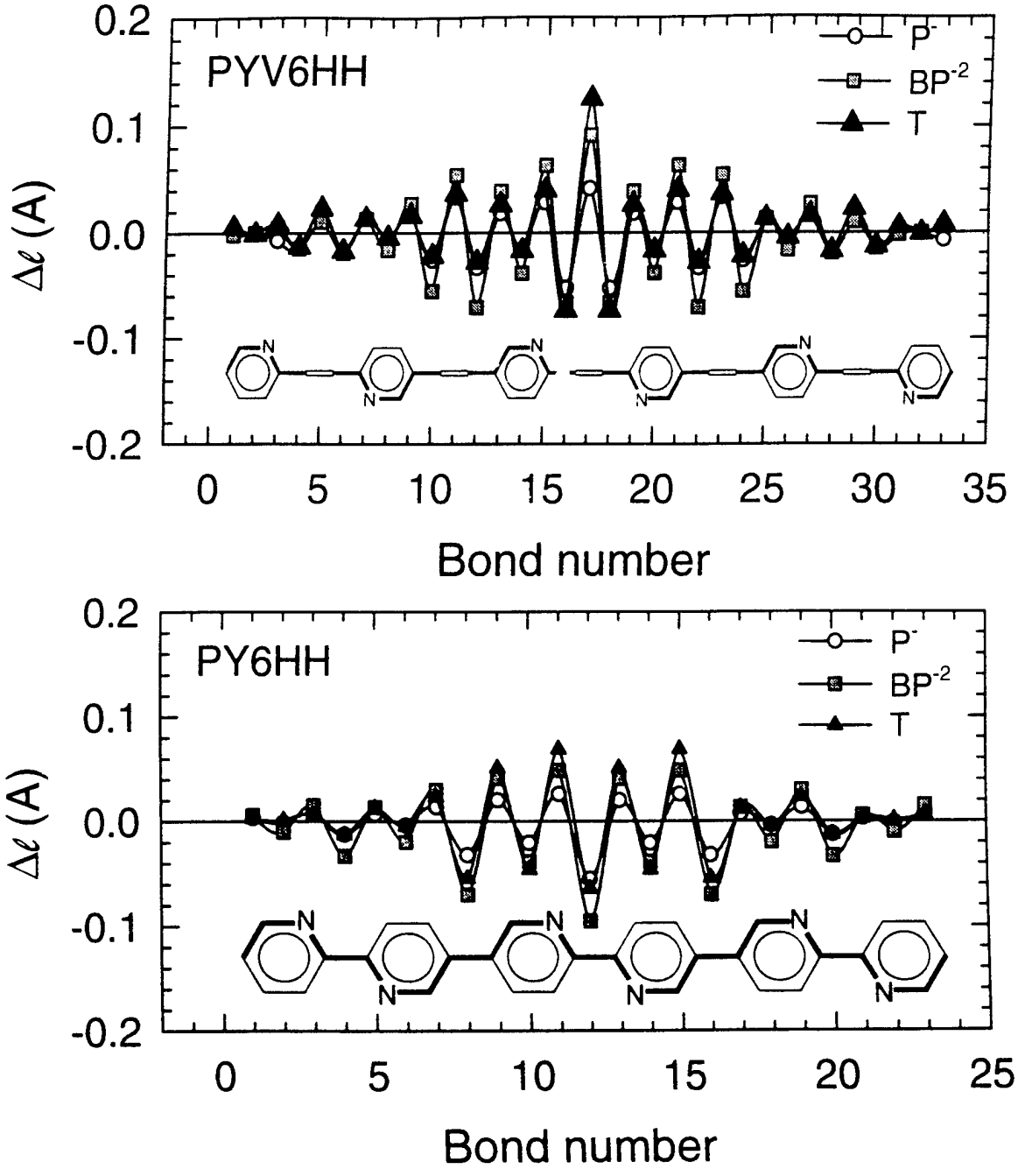


**Figure 3, Blatchford, Gustafson and Epstein**

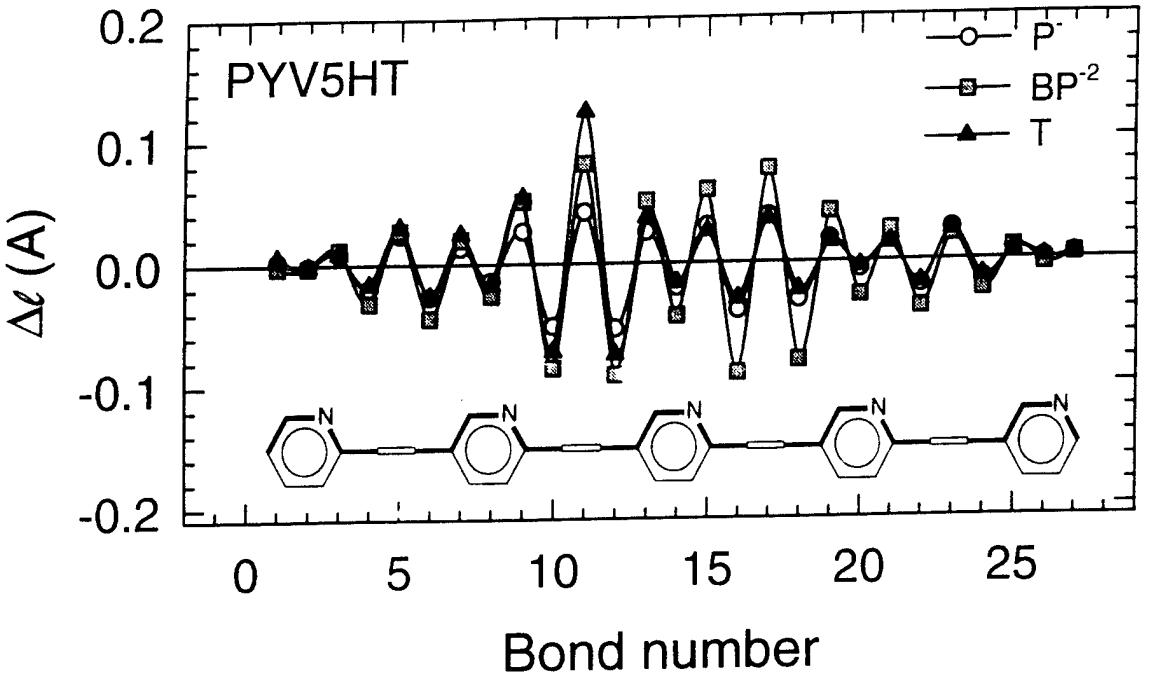


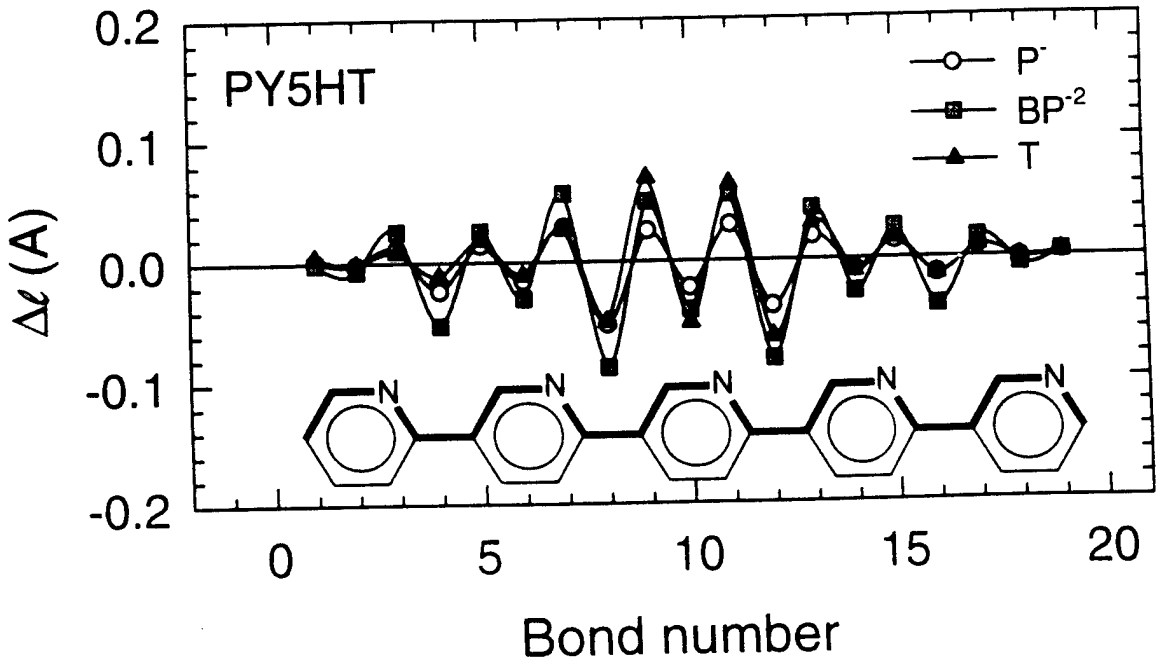


**Figure 4, Blatchford, Gustafson and Epstein**

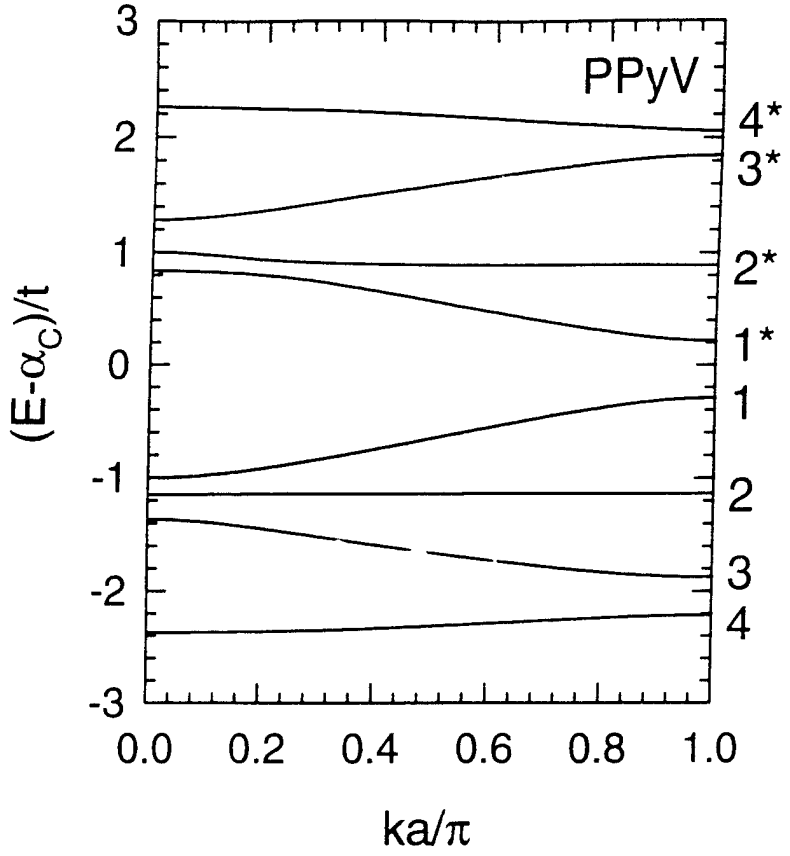


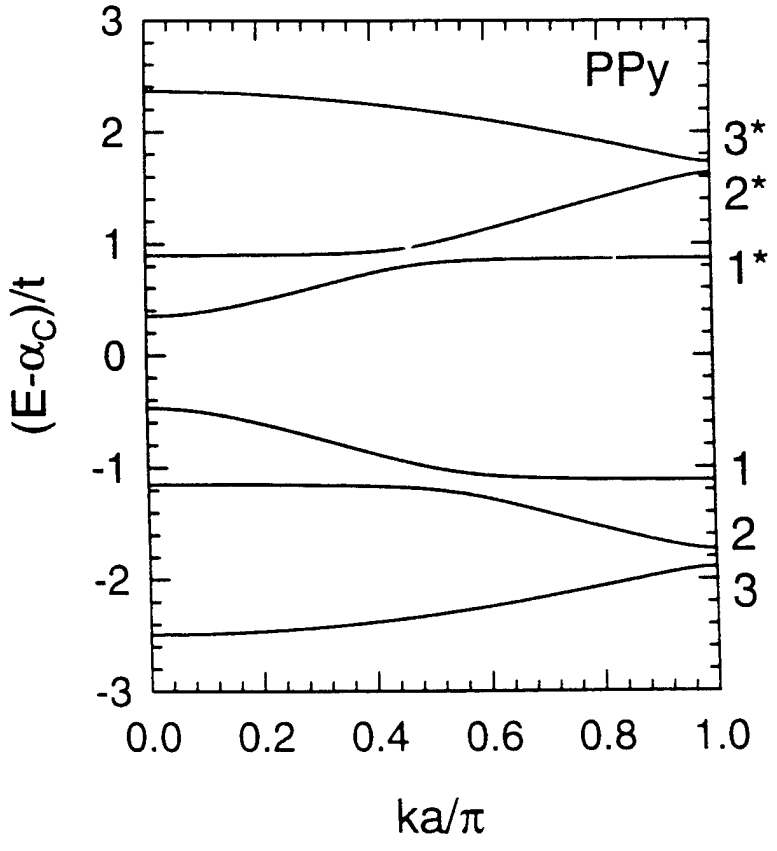


**Figure 5, Blatchford, Gustafson and Epstei**

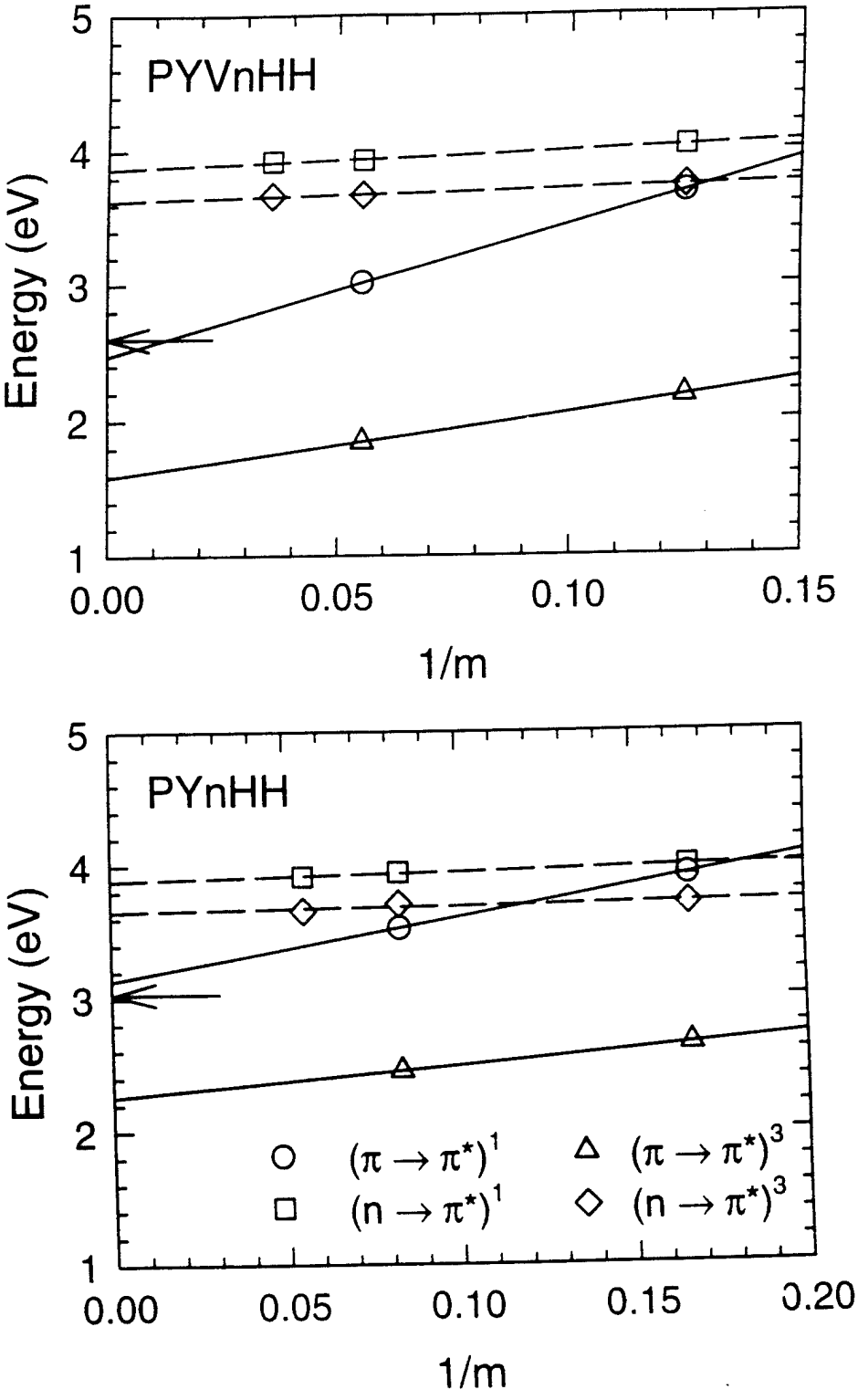


**Figure 6, Blatchford, Gustafson and Epstein**

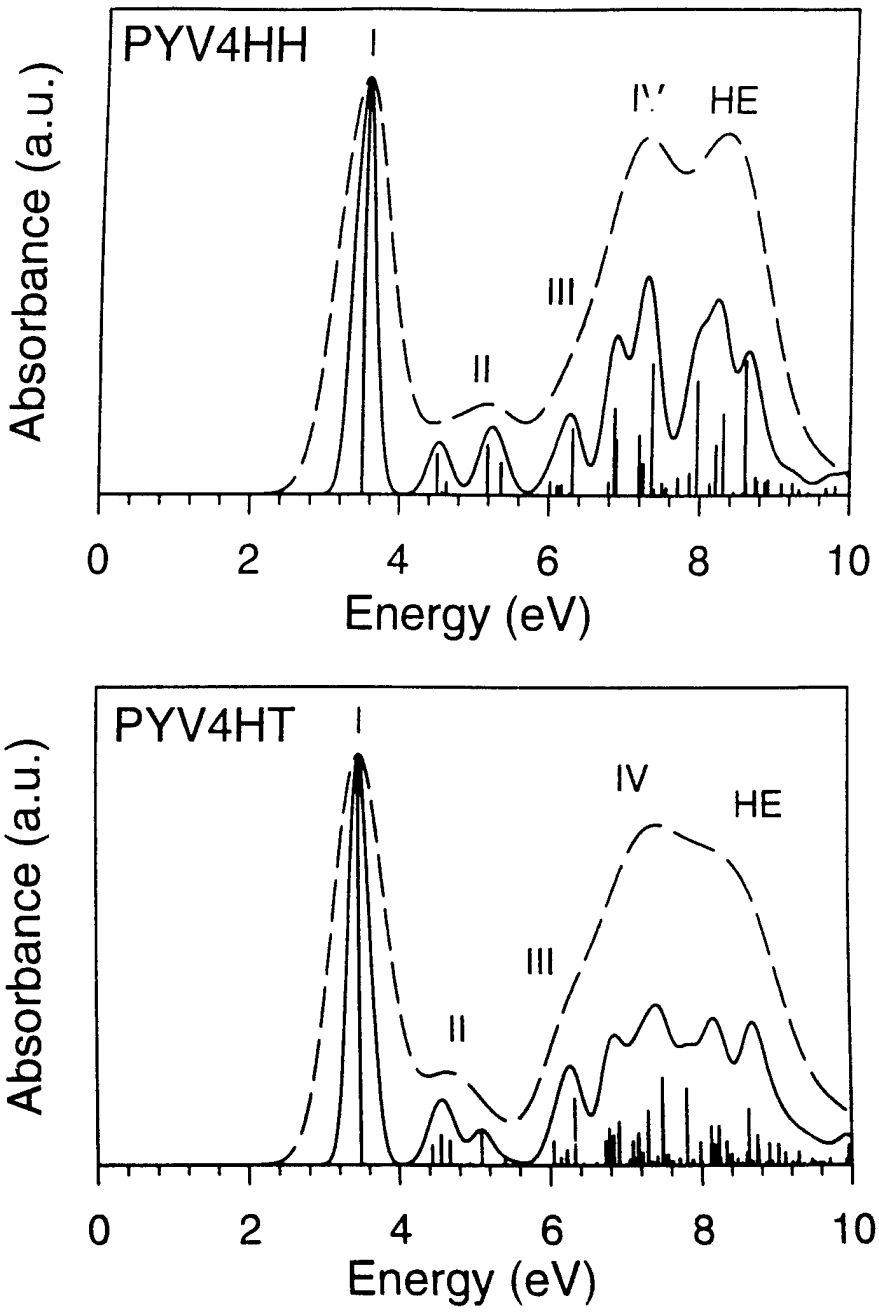


**Figure 7, Blatchford, Gustafson and Epstein**

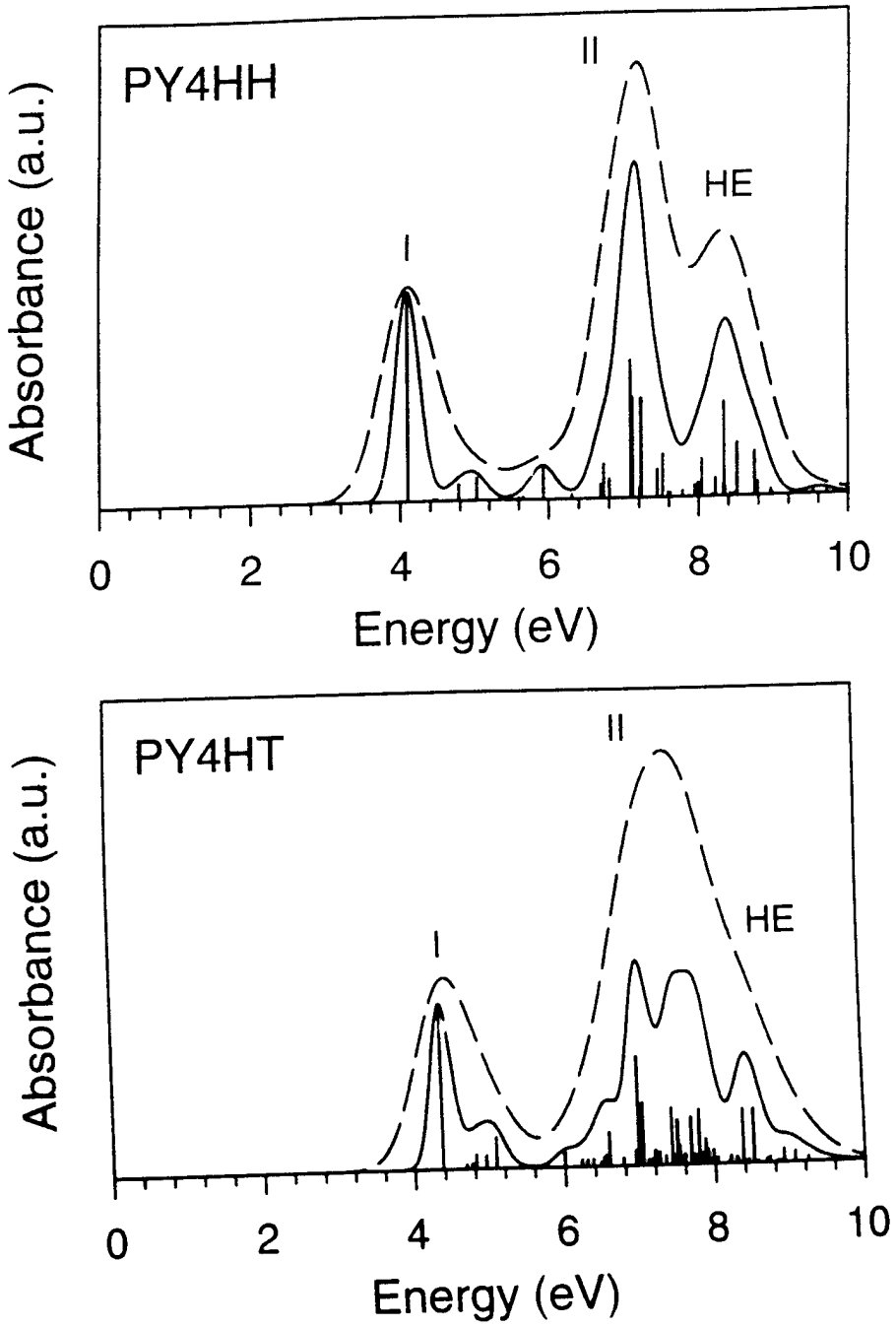


**Figure 8, Blatchford, Gustafson and Epstei**

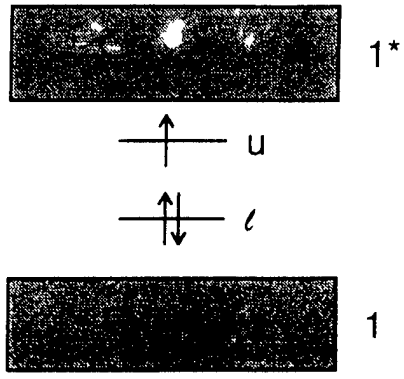


**Figure 9, Blatchford, Gustafson and Epstein**

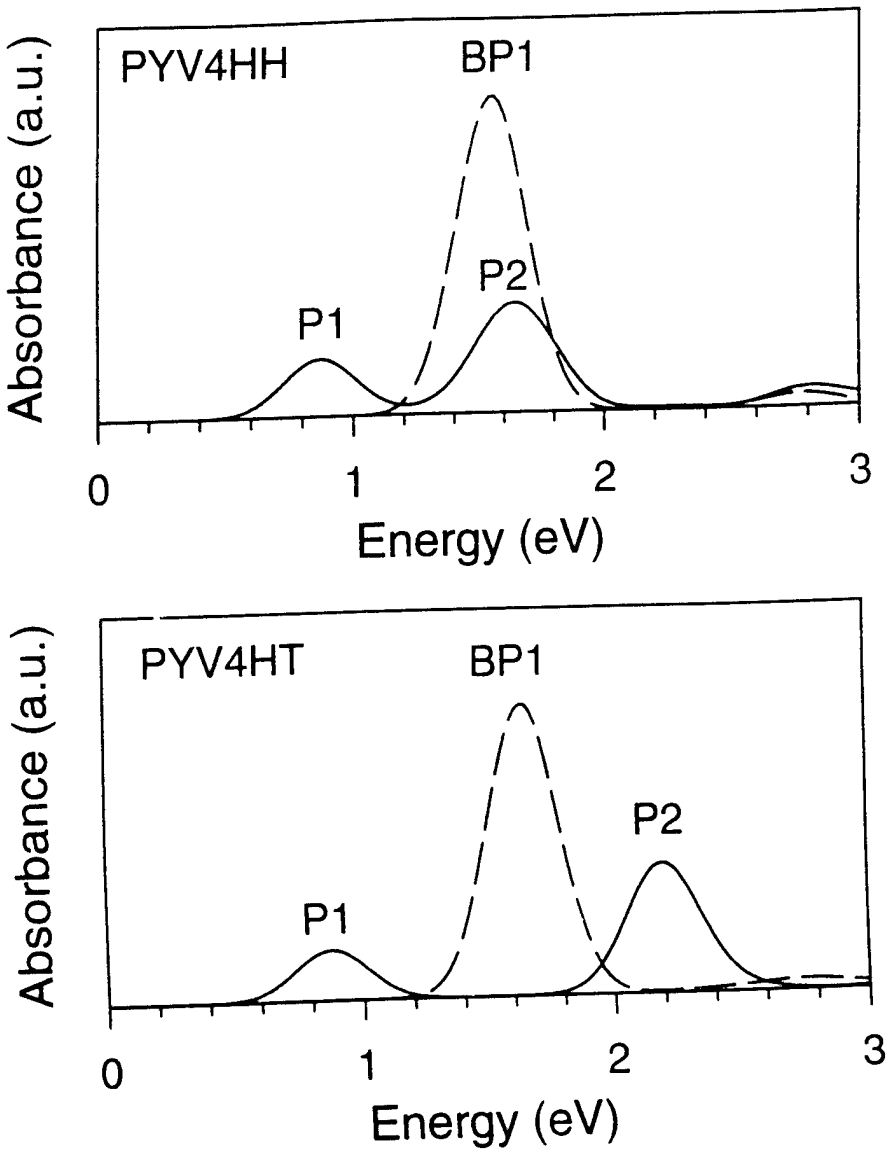


**Figure 10, Blatchford, Gustafson and Epstein**

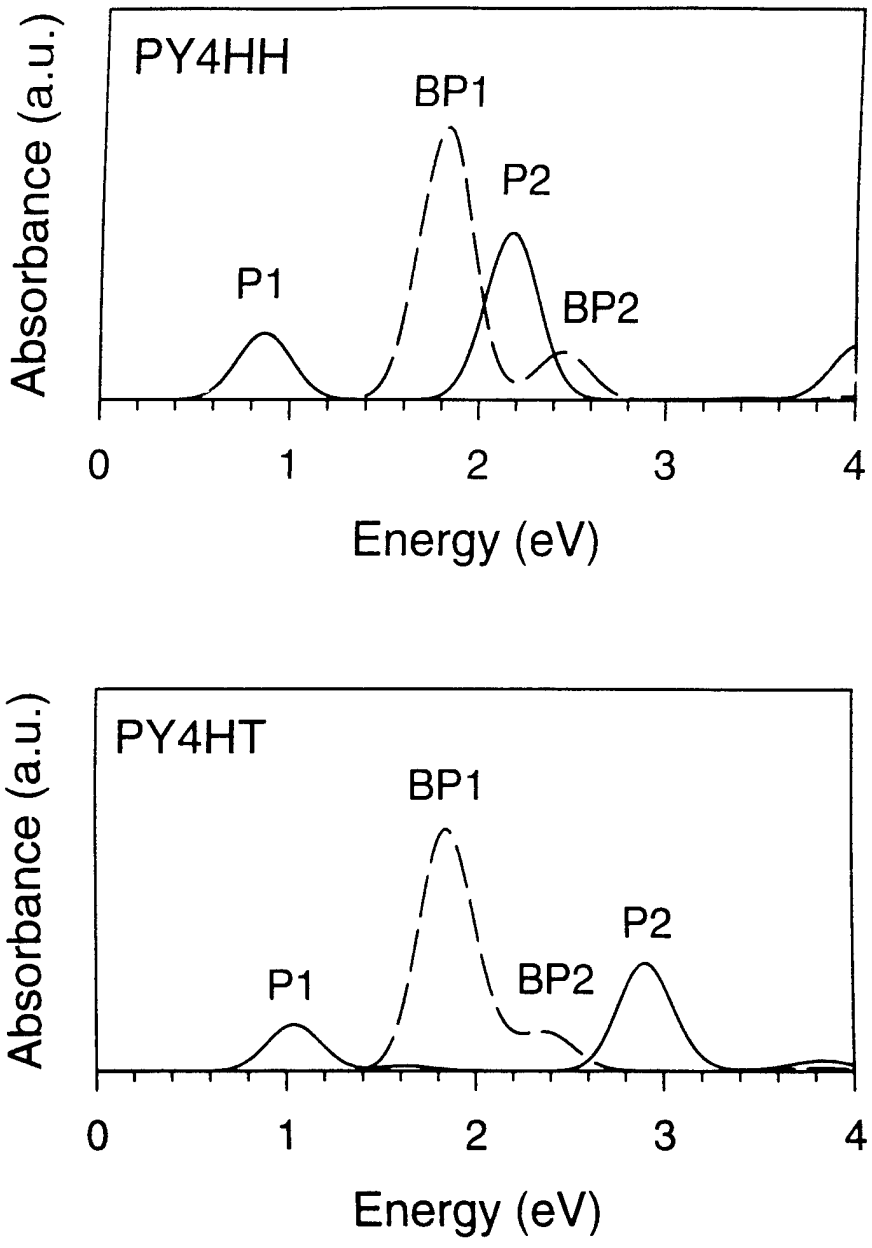


**Figure 11, Blatchford, Gustafson and Epstein**

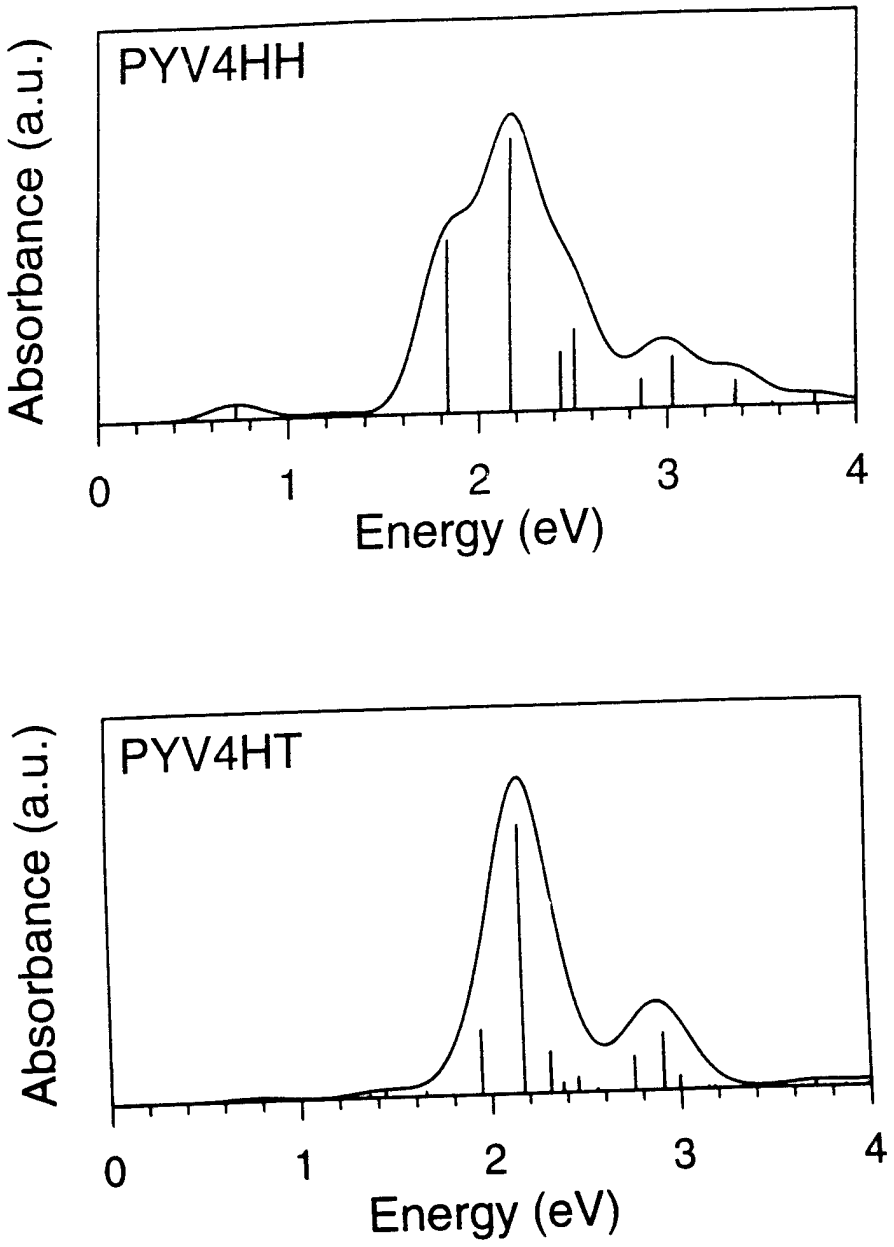


**Figure 12, Blatchford, Gustafson and Epstei**

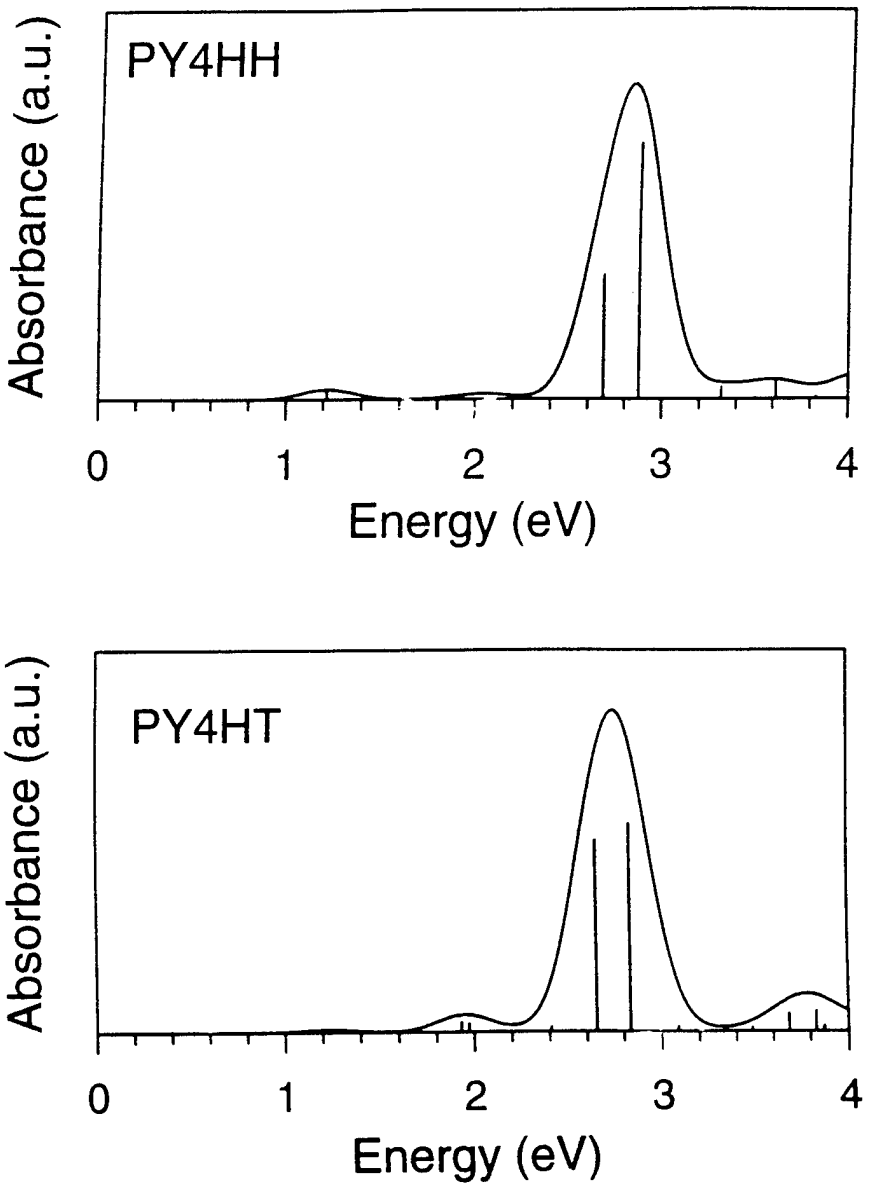


**Figure 13, Blatchford, Gustafson and Epstein**

| Peak | Transition energy (eV) | Pol. | Oscillator Strength | Squared CI Expansion Coefficients |
|---|---|---|---|---|
| I | 3.496 | 16.9 | 2.7514 | 0.97 (1→1*) |
| II | 4.513 | 18.7 | 0.2709 | 0.76 (1→2*) + 0.12 (2→1*) |
| | 4.583 | z | 0.0152 | 0.74 (n→1*) + 0.25 (n→2*) |
| | 4.640 | 71.1 | 0.0808 | 0.65 (1→1*) + 0.19 (1→2*) + 0.06 (2→1*) + 0.05 (2→2*) |
| | 5.186 | 17.3 | 0.3319 | 0.52 (1→2*) + 0.29 (1→1*) + 0.09 (2→1*) |
| | 5.365 | 13.9 | 0.2150 | 0.79 (1→1*) + 0.09 (1→2*) |
| III | 6.016 | 10.3 | 0.0889 | 0.43 (1→2*) + 0.27 (1→1*) + 0.22 (2→1*) |
| | 6.111 | 12.3 | 0.0642 | 0.47 (1→3*) + 0.28 (1→1*) + 0.16 (1→2*) |
| | 6.163 | 57.1 | 0.0667 | 0.33 (1→1*) + 0.28 (1→3*) + 0.23 (2→1*) + 0.09 (1→2*) |
| | 6.271 | 60.2 | 0.0154 | 0.52 (2→1*) + 0.16 (2→1*) + 0.14 (1→1*) + 0.07 (1→3*) + 0.05 (2→2*) |
| | 6.310 | 71.2 | 0.4419 | 0.40 (2→1*) + 0.35 (1→2*) + 0.07 (1→1*) + 0.06 (2→2*) |
| IV | 6.789 | 63.1 | 0.0886 | 0.23 (3→1*) + 0.20 (1→2*) + 0.20 (1→3*) + 0.13 (2→2*) + 0.12 (2→1*) + 0.05 (1→1*) |
| | 6.864 | 43.3 | 0.5761 | 0.35 (2→1*) + 0.25 (1→3*) + 0.20 (1→2*) + 0.07 (2→2*) + 0.06 (1→1*) |
| | 6.890 | 55.9 | 0.3695 | 0.36 (1→3*) + 0.16 (2→2*) + 0.12 (3→1*) + 0.11 (1→2*) + 0.11 (2→1*) + 0.09 (1→1*) |
| | 7.193 | 47.3 | 0.3989 | 0.45 (1→2*) + 0.22 (2→1*) + 0.12 (2→2*) + 0.10 (1→3*) |
| | 7.248 | 53.3 | 0.2100 | 0.34 (2→1*) + 0.23 (2→2*) + 0.16 (1→3*)+ 0.10 (1→2*) + 0.06 (3→1*) + 0.06 (1→1*) |
| | 7.359 | 15.0 | 0.8747 | 0.31 (2→2*) + 0.21 (2→1*) + 0.19 (3→1*) + 0.09 (1→3*) + 0.07 (1→2*) + 0.05 (3→2*) |
| | 7.390 | 11.9 | 0.0419 | 0.29 (1→3*) + 0.22 (1→2*) + 0.13 (1→1*) + 0.12 (3→1*) + 0.10 (2→2*) + 0.07 (2→1*) |
| | 7.497 | 39.5 | 0.0815 | 0.28 (1→3*) + 0.21 (1→2*) + 0.15 (2→2*) + 0.09 (2→1*) + 0.09 (1→1*) + 0.06 (2→3*) + 0.05 (3→2*) |
| | 7.552 | 48.9 | 0.0506 | 0.44 (2→2*) + 0.11 (2→3*) + 0.10 (1→1*) + 0.10 (1→3*) + 0.09 (3→2*) + 0.06 (3→1*) + 0.06 (2→1*) |
| HE | 7.706 | 69.6 | 0.1157 | 0.28 (1→1*) + 0.18 (1→3*) + 0.15 (3→1*) + 0.12 (1→2*) + 0.10 (2→1*) + 0.07 (2→2*) |
| | 7.862 | 85.0 | 0.1466 | 0.37 (2→1*) + 0.16 (3→1*) + 0.15 (1→2*) + 0.11 (2→3*) + 0.11 (2→2*) |
| | 7.958 | 39.2 | 0.7591 | 0.26 (2→1*) + 0.25 (1→2*) + 0.15 (2→2*) + 0.14 (2→3*) + 0.07 (3→2*) + 0.06 (1→3*) |
| | 8.135 | 25.4 | 0.0771 | 0.31 (1→3*) + 0.23 (3→1*) + 0.19 (2→3*) + 0.11 (2→1*) + 0.05 (2→2*) |
| | 8.210 | 32.2 | 0.3322 | 0.23 (1→3*) + 0.18 (3→1*) + 0.16 (2→2*) + 0.08 (3→3*) + 0.10 (2→3*) + 0.08 (2→1*) + 0.08 (3→2*) + 0.06 (1→2*) |

**Table I, Blatchford, Gustafson and Epstein**

| | | | |
|---|---|---|---|
| 8.309 | 63.9 | 0.5434 | 0.31 (2→2*) + 0.24 (2→1*) + 0.23 (3→2*) + 0.06 (3→1*) |
| 8.450 | 60.1 | 0.0173 | 0.34 (1→2*) + 0.28 (2→2*) + 0.11 (2→1*) + 0.09 (3→2*) + 0.07 (1→1*) |
| 8.572 | 79.0 | 0.0162 | 0.28 (2→2*) + 0.26 (2→1*) + 0.24 (3→1*) + 0.14 (2→3*) + 0.08 (3→2*) |
| 8.602 | 83.2 | 0.8939 | 0.21 (1→3*) + 0.18 (3→1*) + 0.17 (2→2*) + 0.16 (3→3*) + 0.14 (2→3*) + 0.08 (2→1*) + 0.06 (3→2*) |
| 8.620 | 38.7 | 0.0769 | 0.43 (2→2*) + 0.24 (1→3*) + 0.12 (2→3*) + 0.07 (1→2*) + 0.05 (3→1*) + 0.05(3→2*) |
| 8.741 | 64.2 | 0.1182 | 0.36 (2→2*) + 0.25 (2→3*) + 0.16 (2→1*) + 0.06 (1→3*) + 0.05 (3→2*) |
| 8.766 | 55.1 | 0.0898 | 0.39 (2→2*) + 0.35 (3→2*) + 0.10 (1→3*) + 0.06 (3→1*) |
| 8.872 | 45.1 | 0.0835 | 0.32 (3→2*) + 0.26 (2→3*) + 0.17 (2→2*) + 0.12 (2→1*) + 0.06 (3→1*) |
| 8.910 | 71.8 | 0.1017 | 0.36 (1 →3*) + 0.18 (3→2*) + 0.14 (2→1*) + 0.14 (3→1*) + 0.12 (3→3*) |
| 9.093 | 62.3 | 0.0720 | 0.35 (1→3*) + 0.34 (2→3*) + 0.10 (2→1*) + 0.06 (3→3*) + 0.06 (2→2*) + 0.05 (3→2*) |
| 9.242 | 61.1 | 0.0775 | 0.37 (3→2*) + 0.17 (2→3*) + 0.10 (1→3*) + 0.11 (2→2*) + 0.10 (2→1*) + 0.05 (3→3*) |
| 9.332 | 62.9 | 0.0325 | 0.29 (2→2*) + 0.28 (3→1*) + 0.20 (2→3*) + 0.06 (2→1*) + 0.05 (3→3*) + 0.05 (1→3*) |
| 9.688 | 58.1 | 0.0420 | 0.61 (2→2*) + 0.16 (3→2*) + 0.08 (2→3*) + 0.07 (3→1*) + 0.05 (2→1*) |
| 9.696 | 65.2 | 0.0324 | 0.26 (2→3*) + 0.18 (3→3*) + 0.18(2→2*) + 0.16 (3→1*) + 0.09 (3→2*) + 0.05 (2→1*) |

**Table I cont'd, Blatchford, Gustafson and Epstein**

| Peak | Transition energy (eV) | Pol. | Oscillator Strength | Squared CI Expansion Coefficients |
|---|---|---|---|---|
| I | 4.100 | 3.8 | 1.7212 | 0.95 (1→1*) |
| | 4.447 | z | 0.0129 | 0.84 (n→1*) + 0.07 (n→2*) + 0.05 (1→1*) |
| | 4.486 | 14.9 | 0.0154 | 0.83 (n→1*) + 0.08 (n →2*) + 0.06 (1→1*) |
| | 4.783 | 24.9 | 0.1294 | 0.77 (1→1*) + 0.10 (2→1*) + 0.06 (2→2*) |
| | 5.026 | 42.7 | 0.1838 | 0.49 (1→2*) + 0.32 (1→1*) + 0.11 (2→1*) + 0.06 (2→2*) |
| | 5.599 | 29.4 | 0.0130 | 0.48 (n→1*) + 0.44 (n→2*) |
| | 5.660 | z | 0.0200 | 0.76 (1→1*) + 0.09 (n→1*) + 0.08 (1→2*) |
| | 5.930 | 35.4 | 0.2712 | 0.60 (1→1*) + 0.29 (1→2*) + 0.05 (2→1*) + 0.05 (n→1*) |
| | 6.310 | 42.9 | 0.0337 | 0.43 (1→2*) + 0.36 (1→1*) + 0.13 (2→1*) |
| | 6.690 | 61.1 | 0.1188 | 0.42 (1→1*) + 0.29 (1→2*) + 0.21 (2→1*) |
| | 6.701 | z | 0.0543 | 0.34 (1→2*) + 0.33 (1→1*) + 0.26 (2→1*) |
| | 6.730 | 84.8 | 0.2833 | 0.51 (1→2*) + 0.28 (2→1*) + 0.13 (1→1*) |
| | 6.804 | 65.1 | 0.1573 | 0.51 (1→1*) + 0.30 (2→1*) + 0.07 (1→2*) + 0.06 (n→1*) |
| II | 7.091 | 16.2 | 1.1261 | 0.39 (n→1*) + 0.19 (2→1*) + 0.16 (1→1*) + 0.15 (2→2*) + 0.10 (n→2*) |
| | 7.115 | 13.1 | 0.8210 | 0.29 (2→1*) + 0.27 (n→1*) + 0.15 (n→2*) + 0.09 (2→2*) + 0.06 (1→2*) + 0.05 (1→1*) |
| | 7.144 | z | 0.0119 | 0.47 (n→1*) + 0.34 (n→2*) + 0.08 (1→2*) + 0.04 (2→1*) |
| | 7.210 | z | 0.0897 | 0.37 (1→2*) + 0.33 (2→1*) + 0.11 (1→1*) + 0.11 (n→1*) |
| | 7.231 | 64.4 | 0.8140 | 0.36 (2→1*) + 0.32 (1→2*) + 0.12 (2→2*) + 0.12 (1→1*) |
| | 7.443 | 68.3 | 0.2265 | 0.29 (n→1*) + 0.24 (n→2*) + 0.16 (2→1*) + 0.13 (1→1*) + 0.07 (2→2*) + 0.09 (1→2*) |
| | 7.515 | 69.3 | 0.3541 | 0.34 (2→1*) + 0.34 (1→1*) + 0.15 (1→2*) + 0.08 (n→2*) |
| | 7.589 | 4.4 | 0.0376 | 0.29 (1→1*) + 0.20 (n→1*) + 0.18 (n→2*) + 0.17 (2→1*) + 0.10 (2→2*) |
| | 7.783 | 79.4 | 0.0484 | 0.27 (n→2*) + 0.27 (1→2*) + 0.13 (n→1*) + 0.12 (1→1*) + 0.10 (2→2*) + 0.09 (2→1*) |
| HE | 7.948 | 46.6 | 0.0959 | 0.28 (2→1*) + 0.21 (n→1*) + 0.20 (1→2*) + 0.13 (n→2*) + 0.09 (2→2*) + 0.06 (1→1*) |
| | 7.988 | 0.9 | 0.1152 | 0.45 (2→1*) + 0.42 (2→2*) + 0.06 (1→1*) |
| | 8.040 | 68.6 | 0.3116 | 0.41 (n→2*) + 0.25 (2→1*) + 0.14 (n→1*) + 0.12 (1→2*) |
| | 8.226 | 64.2 | 0.1460 | 0.28 (1→2*) + 0.22 (2→2*) + 0.16 (2→1*) + 0.14 (1→1*) + 0.10 (n→1*) + 0.07 (n→2*) |
| | 8.331 | 67.6 | 0.0936 | 0.29 (1→2*) + 0.27 (2→1*) + 0.19 (1→1*) + 0.18 (2→2*) |
| | 8.342 | 84.2 | 0.7729 | 0.35 (2→1*) + 0.34 (2→2*) + 0.20 (1→2*) + 0.11 (1→1*) |
| | 8.353 | z | 0.0743 | 0.37 (2→1*) + 0.29 (2→2*) + 0.21 (1→2*) + 0.10 (1→1*) |
| | 8.427 | 66.6 | 0.0180 | 0.64 (n→1*) + 0.28 (n→2*) |
| | 8.479 | z | 0.0238 | 0.27 (1→2*) + 0.24 (2→2*) + 0.20 (n→1*) + 0.12 (1→1*) + 0.11 (2→1*) + 0.06 (n→2*) |
| | 8.514 | 74.8 | 0.4391 | 0.39 (2→1*) + 0.37 (2→2*) + 0.19 (1→2*) |
| | 8.747 | 87.5 | 0.3627 | 0.40 (2→2*) + 0.24 (2→1*) + 0.21 (1→1*) + 0.12 (1→2*) |
| | 8.784 | 60.1 | 0.1131 | 0.41 (1→2*) + 0.26 (2→2*) + 0.25 (2→1*) + 0.06 (1→1*) |
| | 8.962 | 34.7 | 0.0455 | 0.30 (2→2*) + 0.29 (2→1*) + 0.20 (n→2*) + 0.11 (n→1*) + |

**Table II, Blatchford, Gustafson and Epstein**

| | | | |
|---|---|---|---|
| | | | 0.07 (1→2*) |
| 8.981 | 43.1 | 0.2060 | 0.46 (n→2*) + 0.20 (n→1*) + 0.14 (2→2*) + 0.12 (2→1*) + 0.05 (1→2*) |
| 9.532 | 74.2 | 0.0355 | 0.48 (2→2*) + 0.29 (2→1*) + 0.17 (1→2*) |
| 9.711 | 86.3 | 0.0304 | 0.55 (1→2*) + 0.34 (2→2*) + 0.06 (n→2*) |

**Table II cont'd, Blatchford, Gustafson and Epstein**

| Transition energy (eV) | Oscillator Strength | Squared CI Expansion Coefficients |
|---|---|---|
| 0.871 | 0.7266 | 0.61 (u→1*) + 0.16 (u→2*) + 0.11 (3→2*) + 0.05 (u→3*) |
| 1.281 | 0.0625 | 0.89 (u→2*) |
| 1.586 | 0.8837 | 0.24 (ℓ→u) + 0.22 (u→1*) + 0.17 (u→2*) + 0.15 (3→2*) + 0.05 (ℓ→1*) |
| 1.728 | 0.6858 | 0.54 (u→2*) + 0.19 (ℓ→u) + 0.07 (3→2*) |
| 2.283 | 0.0380 | 0.43 (u→3*) + 0.15 (ℓ→2*) + 0.10 (3→3*) + 0.07 (1→3*) |
| 2.783 | 0.1975 | 0.37 (ℓ→u) + 0.36 (3→2*) + 0.06 (u→3*) |
| 2.871 | 0.0557 | 0.39 (3→3*) + 0.15 (ℓ→2*) + 0.10 (3→1*) + 0.08 (u→3*) + 0.06 (ℓ→u) |

**Table III, Blatchford, Gustafson and Epstein**

| Transition energy (eV) | Oscillator Strength | Squared CI Expansion Coefficients |
|---|---|---|
| 1.552 | 4.0342 | 0.90 (u→1*) + 0.06 (ℓ→1*) |
| 2.624 | 0.0318 | 0.80 (u→2*) + 0.12 (ℓ→2*) |
| 2.794 | 0.1549 | 0.62 (u→3*) + 0.28 (u→2*) + 0.06 (ℓ→2*) |

**Table IV, Blatchford, Gustafson and Epstein**

| Transition energy (eV) | Oscillator Strength | Squared CI Expansion Coefficients |
|---|---|---|
| 0.837 | 0.4631 | 0.88 (u→1*) |
| 1.639 | 0.0807 | 0.92 (u→2*) |
| 2.817 | 1.1926 | 0.72 (ℓ→u) + 0.06 (1→1*) |

**Table V, Blatchford, Gustafson and Epstein**

| Transition energy (eV) | Oscillator Strength | Squared CI Expansion Coefficients |
|---|---|---|
| 1.814 | 2.8016 | 0.92 (u→1*) |
| 2.253 | 0.0179 | 0.84 (u→1*) + 0.08 (u→2*) |
| 2.451 | 0.4837 | 0.86 (u→2*) + 0.12 (u→1*) |

**Table VI, Blatchford, Gustafson and Epstein**

| Transition energy (eV) | Oscillator Strength | Squared CI Expansion Coefficients |
|---|---|---|
| 0.726 | 0.0579 | 0.40 (u→1*) + 0.14 (1→ℓ) + 0.11 (ℓ→1*) + 0.08 (1→u)+ 0.07 (u→3*) |
| 1.235 | 0.0150 | 0.79 (u→2*) + 0.07 (ℓ→2*) |
| 1.835 | 0.6606 | 0.18 (ℓ→1*) + 0.24 (1→1*) + 0.11 (u→1*) + 0.10 (u→3*) + 0.07 (n→1*) |
| 2.169 | 1.0450 | 0.25 (u→1*) + 0.15 (ℓ→1*) + 0.14 (ℓ→3*) + 0.11 (u→3*) + 0.05 (ℓ→2*) |
| 2.434 | 0.2195 | 0.39 (1→ℓ) + 0.11 (ℓ→1*) + 0.08 (u→2*) + 0.05 (1→2*) |
| 2.508 | 0.3045 | 0.32 (u→2*) + 0.19 (1→ℓ) + 0.15 (1→2*) + 0.12 (n→2*) + 0.07 (ℓ→2*) |
| 2.860 | 0.1075 | 0.19 (u→3*) + 0.10 (ℓ→1*) + 0.09 (1→u) + 0.09 (1→1*) + 0.06 (u→2*) + 0.05 (n→ℓ) + 0.05 (3→ℓ) + 0.05 (n→1*) + 0.05 (1→2*) + 0.05 (1→3*) |
| 3.027 | 0.1909 | 0.18 (1→u) + 0.14 (u→3*) + 0.07 (ℓ→7*) + 0.13 (1→3*) + 0.06 (3→1*) + 0.05 (1→1*) + 0.05 (n→2*) |

**Table VII, Blatchford, Gustafson and Epstein**

| Transition energy (eV) | Oscillator Strength | Squared CI Expansion Coefficients |
|---|---|---|
| 1.141 | 0.0325 | 0.60 (u→1*) + 0.24 (1→ℓ) + 0.05 (u→2*) |
| 1.959 | 0.0702 | 0.59 (u→2*) + 0.23 (u→1*) + 0.07 (1→ℓ) |
| 2.101 | 0.0226 | 0.50 (u→1*) + 0.37 (u→2*) + 0.05 (ℓ→1*) |
| 2.717 | 0.6636 | 0.33 (u→1*) +0.32 (u→2*) + 0.18 (ℓ→1*) + 0.05 (n→ℓ) |
| 2.906 | 1.2306 | 0.39 (u→2*) + 0.35 (1→ℓ) + 0.14 (u→1*) |
| 3.330 | 0.0601 | 0.49 (u→1*) + 0.11 (u→2*) + 0.09 (ℓ→1*) + 0.07 (1→1*) + 0.06 (1→2*) |
| 3.501 | 0.6221 | 0.51 (2→ℓ) + 0.11 (ℓ→1*) + 0.05 (u→2*) + 0.05 (1→1*) |

**Table VIII, Blatchford, Gustafson and Epstein**